Charge transition levels of carbon-, oxygen-, and hydrogen-related defects at the SiC/SiO_2 interface through hybrid functionals

Fabien Devynck, Audrius Alkauskas, Peter Broqvist, and Alfredo Pasquarello
Chaire de Simulation à l'Echelle Atomique (CSEA), Ecole Polytechnique Fédérale de Lausanne (EPFL), CH-1015 Lausanne, Switzerland

(Received 11 August 2011; revised manuscript received 3 November 2011; published 29 December 2011)

We calculate charge transition levels of various defects at the SiC/SiO_2 interface within a scheme based on hybrid density functionals, which accurately reproduce the involved band gaps and band offsets. The defect levels are first evaluated in bulk models of the interface components and then aligned with respect to the interface band diagram through the use of a model interface showing good structural and electronic properties. Interface-specific polarization effects are evaluated separately through classical electrostatics. We considered carbon-related defects involving single atoms and dimers in both the crystalline SiC substrate and the amorphous SiO_2 oxide. Our investigation also comprises oxygen- and hydrogen-related defects, including the Si-Si bond (O vacancy), the Si_2-C-O structure, the peroxy linkage, and the hydrogen bridge (Si-H-Si). Among the defects studied, the Si_2-C-O structure represents the best candidate for the high defect density measured near the conduction band of SiC.

DOI: 10.1103/PhysRevB.84.235320 PACS number(s): 68.35.Ct, 73.20.−r, 71.15.Pd

I. INTRODUCTION

With its wide band gap, high thermal conductivity, high saturated electron drift velocity, and high breakdown electric field, silicon carbide (SiC) is the candidate of choice for high-temperature, high-power, high-frequency, and high-speed electronic devices.[1] Despite these remarkable bulk properties, SiC-based devices are still facing many performance challenges due to the high density of defect states (D_{it}) at the SiC/SiO_2 interface, which remains up to two orders of magnitude larger than at Si/SiO_2 interfaces.[2–6] The literature suggests that two main classes of defects contribute to the distribution of the D_{it} across the SiC band gap. On the one hand, a first class of defects spans the entire SiC band gap with a density not exceeding 10^{12} cm^{-2} eV^{-1}. Several distinct peaks and shoulders of D_{it} could be identified,[4,7–9] the positions of which may slightly vary depending on the growth method, the applied measurement method, and the polytype under study. On the other hand, a second class of defects consists of electron traps in the upper half of the band gap giving rise to a peak reaching 10^{13} cm^{-2} eV^{-1} near the $4H$-SiC conduction band. The atomic-scale nature of these defects has not yet clearly been established.

During thermal oxidation of SiC, most of the excess carbon is believed to be removed from the interface through the formation and diffusion of CO molecules in the oxide. However, some of the carbon can remain in the oxide and form carbon clusters or graphitic regions. Some insight into the nature of the interface defects comes from electron spin resonance experiments on oxidized porous SiC, which identified sp^3 carbon dangling bonds.[10] Graphite-like clusters and sp^2-bonded carbon atoms as observed in amorphous carbon were also proposed to be predominantly responsible for the high defect state density.[4] Comparison between internal photoemission spectra of oxidized SiC and amorphous, hydrogenated carbon films deposited onto SiO_2 suggested that small, π-bonded carbon clusters are responsible for the interface states observed in the lower part of the SiC band gap, while larger carbon islands give rise to a graphite-like band structure, responsible for some of the traps near the band edges.[4] The presence of interfacial carbon clusters was inferred by atomic-force microscopy experiments revealing nanometer-sized platelet-shaped inhomogeneities at the interface[11] and electron energy loss spectroscopy probing an interfacial 10–15 Å thick C-rich region.[12] Subsequently, surface-sensitized Raman spectroscopy (SERS) measurements claimed the identification of nanographitic structures and polyenes at the interface.[13] The size of the graphitic structures was estimated to be $\leqslant 2$ nm. The authors thus suggested that such carbon structures could be responsible for the interface states.[13] However, this assignment was later questioned.[14] X-ray photoelectron spectroscopy (XPS) also detected graphitic regions at the SiC surface prior to oxidation, but these regions dissolved during *in situ* oxidation and no form of graphite could finally be found at the SiC/SiO_2 interface.[15,16] In summary, there is a general agreement that some interface states, predominantly in the lower part of the SiC band gap, are due to excess carbon at the interface. On the contrary, the presence of large graphitic clusters has not clearly been established. However, carbon-only structures may not fully account for the D_{it} in the lower and mid parts of the band gap. Indeed, XPS measurements[17,18] indicate that the interfacial layer also contains Si-O-C linkages,[15,17] and Si-Si bonds,[18] as well as vacancies surrounded by oxygen.[19]

Intrinsic defects in SiO_2 (Refs. 6,20–23) have been proposed to account for the D_{it} in the upper band gap. Using photon stimulated tunneling (PST), Afanas'ev *et al.* detected oxide defects located close to the interface and suggested that these defects are responsible for the observed mobility degradation.[21,22] PST measurements on SiC devices revealed a mean energy barrier of 2.8 eV,[21,22] indicating that these negatively charged near-interface trap (NIT) levels are positioned 0.1 eV below the conduction band of $4H$-SiC. Similar experiments on Si-based MOS structures located NITs at the same energy level with respect to the conduction band of SiO_2 and with a density comparable to that found in the case of SiC. This corroborated the attribution of these traps to defects of the oxide, probably related to (H-complexed) oxygen vacancies.[20,23] Schörner *et al.* performed capacitance-voltage measurements of n-type MOS

 ©2011 American Physical Society

structures based on 4H-SiC, 6H-SiC, and 15R-SiC.[24] PST and capacitance-voltage experiments are generally not expected to measure the same defect energy levels. Nevertheless, Schörner *et al.* also found defect levels close to the SiC conduction band and concluded that these levels would be responsible for the low inversion channel mobility in 4H-SiC.[24] These defects were suggested to be inherent to all SiC polytypes and energetically pinned at ~2.9 eV above the SiC valence band.[24] In this view, the interface traps would become resonant with the SiC conduction-band states for the polytypes with band gaps smaller than 4H-SiC, e.g., 6H- and 15R-SiC, thereby explaining the lower D_{it} and higher inversion layer mobility of 6H- and 15R-SiC MOS structures compared to 4H-SiC MOS structures. It was demonstrated using constant-capacitance deep level transient spectroscopy (CCDLTS) that the electron-capture cross sections of these interface traps are small and vary over several orders of magnitude, suggesting that a large portion of the traps is located not at the interface but at some distance into the oxide.[25] These NITs were subsequently observed on SiC-based MOS structures grown on different SiC polytypes, on different crystal orientations, and with various oxidation conditions.[26–28] In a subsequent study, Ólafsson *et al.* applied the thermally stimulated current (TSC) technique to investigate the high density of shallow traps near the 4H-SiC/SiO_2 interface. The TSC spectra revealed two distinguishable peaks, thereby indicating that the high D_{it} close to the SiC conduction band may result from different types of defects.[29] More recently, CCDLTS and double CCDLTS of as-oxidized 4H-SiC/SiO_2 interfaces were used to show that the D_{it} near the SiC conduction band consists of several overlapping distributions of interface states distinguished by their different capture cross sections.[30,31]

Numerous treatments have been applied to SiC/SiO_2 interfaces in order to improve their quality, with different outcomes and suggestions regarding the origin of the D_{it}. Reoxidation (a post-oxidation heat treatment in oxygen below oxidation temperature) was shown to have a double-fold effect: a significant decrease in the D_{it} in the lower half of the band gap, but also a slight increase in the D_{it} in the upper part of the band gap.[7] In contrast with Si/SiO_2 interfaces, annealing in H_2 up to 400 °C does not lead to any appreciable passivation of these interface defects, suggesting that dangling bonds give an insignificant contribution to the D_{it}.[4,5] However, partial passivation of interface states could be achieved by nitridation, either by post-oxidation annealing[3,7,32–35] or by oxidation in a gas mixture containing nitrogen.[6,36,37] NO has proven to be the most effective nitrogen precursor; because of safety reasons, N_2O is more often used, but its effectiveness is also attributed to its dissociation into NO. As NO itself can dissociate, atomic oxygen was also proposed to have an effect on the interface state density reduction. Oxidation in an ozone gas ambient containing O_3 molecules thermally dissociating into atomic oxygen led indeed to a significant reduction in the D_{it}. Atomic nitrogen was also shown to be effective in the form of a radical irradiation[38] or by nitrogen implantation prior to oxidation.[39] Recently, it was shown that a post-oxidation anneal in nitric oxide followed by a post-metallization anneal in hydrogen through a platinum gate known to catalyze atomic hydrogen formation resulted in a reduction of the trap density by over an order of magnitude near the conduction band.[40,41] It was suggested that this treatment could eliminate the threefold-coordinated atoms responsible for the high interface trap density either by hydrogen passivation or by nitrogen replacement.[41,42] XPS investigations also led to the proposal that nitrogen could dissolve carbon clusters, leading to the removal of carbon from the interface.[43,44] Nitrogen could also saturate Si dangling bonds and replace oxygen in strained Si-O-Si bonds.[44] Overall, nitridation seems to affect both the D_{it} in the lower and upper parts of the band gap, with a more effective reduction of the latter.[6] Recently, oxidation in an alumina environment instead of conventional quartz was shown to enhance the mobility at the grown interfaces even further than nitridation.[45] It was first proposed that metallic impurities introduced during the growth in the alumina environment were responsible for this effect;[46] however, it was then demonstrated that the reduction of the NITs was correlated with enhanced oxide growth[47] due to sodium originating from sintered alumina.[48] However, the gate oxide of these devices contains metal impurities causing adverse effects, such as high threshold voltage shifts[47] and sensitivity to bias temperature stress.[49] Overall, the reoxidation or passivation treatments do not provide tangible evidence toward the identification of a class of defects.

Recent density functional calculations provided insight on the nature of typical defects occurring at the SiC/SiO_2 interface. Knaup *et al.* studied the oxidation mechanism of 4H-SiC and typical defects occurring on the semiconductor side of the interface.[50] While the identified defects closely correspond to the D_{it} in the lower part of the SiC band gap, the defects responsible for the high D_{it} close to the conduction band remained unexplained. In a subsequent work, Knaup *et al.* then considered both intrinsic and C-related defects on the oxide side of the interface.[51] In particular, these authors identified Si interstitials and doubly bonded C-C dimers as possible defects in the oxide on the basis of their energy levels in the SiC band gap. However, these defects could not fully account for the photon-stimulated tunneling measurements, indicating similar defect concentrations at Si/SiO_2 and SiC/SiO_2 interfaces.[21,22] Very recently, Wang *et al.* reconsidered possible origins of the high D_{it} in the SiC band gap.[52] Correlated C dangling bonds were proposed as the primary cause for the observed D_{it}, their passivation by H_2 being hindered because of their opposed orientations.[52] However, the calculated levels were located about 1 eV below the SiC conduction-band edge, thereby ruling them out as possible candidates for the D_{it} close to the conduction band. In a previous study, we investigated carbon single-atom and pair defects at the SiC/SiO_2 interface.[53] Our results indicated that such defects concurrently contribute to the defect density in the low and mid parts of the SiC band gap and near the SiC conduction band, establishing a strong correlation between the defect densities in these energy ranges. Moreover, this study showed that the contribution of these carbon defects to the defect density is expected to consist of broad peaks because of the sensitivity to the local structure and environment. Thus, the origin of the intense and narrow peak observed experimentally in the vicinity of the SiC conduction band and uncorrelated with any significant defect density in the lower part of the SiC band gap could not be assigned.[53]

Density functional calculations are indeed a powerful tool to investigate the nature of defects at the SiC/SiO_2 interface. However, the accuracy of such calculations relies on crucial requisites, and some difficulties can be encountered when focusing on interfacial systems. The first requirement is an accurate description of band gaps and band offsets. Yet, standard density functionals are known to give a poor description of these electronic properties. Second, Kohn-Sham energy levels are often used to predict defect levels. However, their physical significance is questionable. It is preferable to describe defect levels through the determination of charge transition levels, which are based on total-energy differences. Indeed, significant quantitative differences might occur between Kohn-Sham levels and charge transition levels of possible defects occurring at the SiC/SiO_2 interface.[51,53] However, the treatment of charged defects at interfaces through periodic slab configurations is particularly challenging as the spurious electrostatic contributions at the interface between different dielectric materials can not trivially be estimated.

In this paper, we determine charge transition levels for a set of defects at the SiC/SiO_2 interface. The considered set comprises various defects invoked in previous literature, including carbon-, oxygen-, and hydrogen-related defects on both the substrate and the oxide sides of the interface. We use a scheme based on hybrid density functionals[54] that gives an accurate description of the involved band gaps and band offsets.[55] To overcome the problem of dealing with charged defects at the interface, we first calculate charge transition levels in bulk models of the interface components. The defect levels are subsequently located within a band diagram of the interface through the use of an atomistic model structure of the SiC/SiO_2 interface.[56] Polarization effects due to the interface are estimated through classical electrostatics. A preliminary and partial account of some of the results in this paper was presented in Ref. 57.

This paper is organized as follows. Section II is devoted to the description of the methods and atomistic models used in this work. In Secs. III, IV, and V, we consider carbon-, oxygen-, and hydrogen-related defects, respectively. The conclusions are drawn in Sec. V. The Appendix comprises a comparison between Kohn-Sham energy levels and charge transition levels.

II. METHODS AND MODELS

A. Computational setup

We describe the electronic structure using a spin-dependent plane-wave pseudopotential scheme based on the generalized gradient approximation proposed by Perdew, Burke, and Ernzerhof (PBE).[58] A plane-wave basis set with a cutoff energy of 70 Ry is used for the wave functions of the valence electrons. In all calculations, core-valence interactions are described by norm-conserving PBE pseudopotentials.[59] A full structural relaxation at the PBE level is performed for each model. The electronic properties are then addressed using hybrid PBE density functionals[54] to achieve an improved description of band gaps.[60,61] In these functionals, a fraction of the PBE exchange interaction is replaced by nonlocal Fock exchange. Following a recently proposed approach,[55] the fraction of Fock exchange included in bulk material calculations is tuned to recover the experimental band gap. The fraction α of included Fock exchange will be denoted in parentheses after the functional acronym, i.e., PBE(α), for notation convenience. We take care of the integrable divergence of the exchange term, thus enabling Γ-point sampling.[62] We here use the CPMD package.[63]

B. Atomistic models

We consider in this work both the $4H$-SiC/SiO_2 and the $6H$-SiC/SiO_2 interfaces. We first study for reference the components of the interfaces in their bulk phase, i.e., crystalline $4H$-SiC, crystalline $6H$-SiC, and amorphous SiO_2. The models of $4H$-SiC and $6H$-SiC, a 96-atom and a 144-atom structure, respectively, were presented in a previous study.[53] The $4H$-SiC and $6H$-SiC Kohn-Sham band gaps calculated at the PBE level (2.2 and 2.0 eV, respectively) severely underestimate the experimental values (3.3 and 3.0 eV, Ref. 1), as usual at this level of theory. At variance, a hybrid functional calculation including 15% of nonlocal Fock exchange results in the valence-band edge going down by $\sim$0.6 eV with respect to the electrostatic potential and the conduction-band edge going up by $\sim$0.4 eV. This fraction of Fock exchange thus essentially yields the experimental band gap for both SiC polytypes.

For amorphous SiO_2, we consider two models consisting of chemically ordered networks of corner-sharing tetrahedra at the experimental density of 2.2 g/cm^3. The smaller model contains 72 atoms and was obtained previously by *ab initio* molecular dynamics.[64] The second model was generated through the sequential use of classical and *ab initio* molecular dynamics.[65] The two models essentially differ by the presence of a larger concentration of three-membered rings in the 72-atom model. The average Si-O-Si bond angle in the 72-atom model slightly underestimates (by $\sim$8%) the experimental value (151°, Ref. 66), while this property is well reproduced in the 144-atom model. At the PBE level of theory, the calculated band gaps are 5.3 and 5.4 eV for the 72-atom and the 144-atom models, respectively. The experimental band gap of 8.9 eV is recovered for a hybrid PBE calculation including 35% of Fock exchange.

We also consider an α-quartz crystalline model of SiO_2. This model contains 72 atoms in an orthorhombic supercell of dimensions $9.95 \times 8.63 \times 10.9$ Å^3. The structure shows a mean Si-O bond length of 1.65 Å and a Si-O-Si angle of 144°. The calculated band gaps are 5.7 and 9.2 eV at the PBE and PBE(0.35) levels of theory, respectively.

The $4H$-SiC/SiO_2 model interface used here was generated previously through a sequential scheme involving classical molecular dynamics and density functional calculations.[56] Our model contains a crystalline substrate with eight planes of alternating Si and C atoms (8.2 Å thick) connected without any coordination defect to an amorphous oxide layer with a thickness of 16 Å. The model structure shows good structural parameters and an oxide density typical of amorphous SiO_2.[56] The $6H$-SiC/SiO_2 model interface was then generated by substituting the 8-plane $4H$-SiC substrate with a 12-plane $6H$-SiC substrate and allowing the structure to relax further.

C. Alignment

Via the use of a hybrid functional with a fixed fraction of Fock exchange, it is not possible to recover the experimental

band gaps for both interface components. Indeed, the use of $\alpha = 15\%$ required for SiC is inappropriate for the band gap of SiO_2, which is reproduced with $\alpha = 35\%$. Furthermore, the interface calculations described suffer from the quantum confinement effect due to the finite thickness of the SiC slab.[56] To circumvent these limitations, we generalize a well-known scheme in which the interface components are described by bulk models with properly aligned electronic structures.[67,68] To reproduce the experimental band gaps of both interface components, the fraction of Fock exchange is separately adjusted in the hybrid functional calculations of the bulk models of the two interface components.[55] In each bulk calculation, the band extrema are first determined with respect to the electrostatic potential and then aligned in an interface band diagram according to the offset of the electrostatic potential derived from the interface calculation. In the model of amorphous SiO_2, the average electrostatic potential is subject to fluctuations due to the disorder and we therefore use the oxygen $2s$ states for the alignment. The reliability of the present scheme rests on the fact that the electrostatic potential across the interface does not depend sensitively on the fraction of Fock exchange used.[55] Indeed, the difference between the average electrostatic potential offset across the SiC/SiO_2 interface in PBE(0.15) and PBE(0.35) calculations does not exceed 0.1 eV. The validity of this scheme is strengthened by the generally very good agreement with experiment that is found for band offsets.[55] For the $4H$-SiC/SiO_2 interface model, we derive valence- and conduction-band offsets of 3.0 and 2.6 eV, respectively, in excellent agreement with their experimental counterparts of 2.9 and 2.7 eV.[1] For the $6H$-SiC/SiO_2 interface model, a similar agreement is found with calculated valence- and conduction-band offsets of 3.0 and 2.9 eV, respectively, comparing well with the respective experimental values of 2.9 and 3.0 eV.[1] These results are graphically illustrated in Fig. 1.

The adopted scheme is particularly useful in the study of defects for which the alignment to the band edges is a critical issue. In particular, it is important to stress that, unlike the band edges, the positions of the defect levels with respect to the average electrostatic potential are essentially independent of the adopted fraction of nonlocal Fock exchange.[69,70] This implies that the different fractions used for the two interface components do not affect the relative positions of defect energy levels associated to defects situated on opposite sides of the interface. The present description offers the advantage of situating the defect levels in an interfacial band diagram, which closely reproduces the experimental one. Such an alignment scheme has already led to several studies in which relative energies of defect levels of various charge states in different interface components are obtained.[71–77]

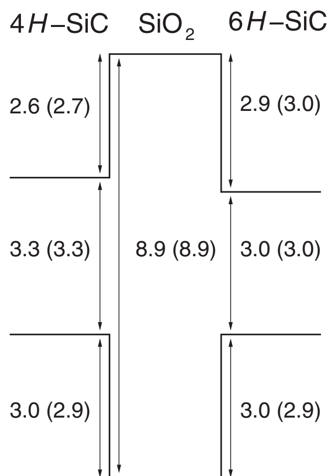

FIG. 1. Interfacial band alignments at the $4H$-SiC/SiO_2 and $6H$-SiC/SiO_2 interfaces, as found in our theoretical scheme. The scheme reproduces the experimental band gaps by construction, but the band offsets are a result of the calculations. Corresponding experimental values from Ref. 1 are given in parentheses. Energies are given in eV.

In the following, the defect levels are given within a band diagram for the $4H$-SiC polytype, which shows the largest band gap among the two polytypes. In case the defects need to be referred to the band edges of $6H$-SiC, these can be found by displacing the conduction-band edge of $4H$-SiC by -0.3 eV (cf. Fig. 1).

In this work, the band bending due to space-charge effects[78] is neglected. Indeed, for the typical density of fixed charge at SiC/SiO_2 interfaces, $\sim 10^{12}$ cm^{-2},[79] band-bending effects occur over several hundred or thousands of angstroms. It is understood that the defects considered in this work are located at distances from the interface for which this effect is negligible.

D. Defect levels

In this work, the various investigated defects are generally generated in the 96-atom model of $4H$-SiC or in the 72-atom model of SiO_2, unless mentioned otherwise. The formation energy of a defect state with charge q is determined as a function of the electron chemical potential μ with respect to the edge of the valence band ϵ_v of the defect-free system as

$$E_f^q(\mu) = E^q - E^0 + q(\epsilon_v + \mu + \Delta V) + E_{\text{corr}}, \quad (1)$$

where E^q and E^0 are the total energies for the defect with charge q and the neutral defect, respectively. ΔV is required for the accurate positioning of the valence band by aligning the electrostatic potential far from the defect to that of the defect-free bulk model.[80] E_{corr} is a correction that accounts for the spurious electrostatic interactions of the charged defect occurring when periodic boundary conditions are used.

When periodic boundary conditions are used, the defect charge is compensated by a uniform background in order to avoid the divergence of the electrostatic energy of the system. Such a periodic system gives rise to spurious electrostatic effects resulting from both the background charge and the image charges. The energetics appropriate to an isolated defect are recovered in the limit of large supercell through a slow convergence.[81] Hence, several electrostatic correction schemes have been proposed,[82–85] but no consensus has yet been reached on the best methodology. In this work, we use the monopole term of the correction proposed by Makov and Payne.[82] For defects in SiC, we use a dielectric constant of 9.6 (Ref. 1), giving rise in our 96-atom model to corrections of $E_{\text{corr}}^{\text{SiC}} = 0.21$ eV and $E_{\text{corr}}^{\text{SiC}} = 0.84$ eV for charges $|q| = 1$ and 2, respectively. For defects in SiO_2, we use a dielectric constant of 4.0, leading in our 72-atom model to $E_{\text{corr}}^{\text{SiO}_2} = 0.5$ eV and $E_{\text{corr}}^{\text{SiO}_2} = 2.0$ eV for $|q| = 1$ and 2, respectively.

The advantage of this correction is that it is simple and that the uncorrected result can easily be recovered. However, the adopted Makov-Payne correction has been found to overcorrect in some cases.[81] This might give rise to inaccuracies, especially in the case of high charge states ($|q| = 2$). In fact, in the attempt of going beyond the monopole term, Lany and Zunger found that the Makov-Payne correction should be scaled to about two thirds of its value.[83] Comparing the two schemes allows one to obtain an estimate of residual inaccuracies. Such effects are more significant for oxide defects. For the SiO_2 defects studied in this work, the largest inaccuracies correspond to $+1/+2$ ($-1/-2$) charge transition levels, with Lany-Zunger corrected values higher (lower) by 0.5 eV with respect to the Makov-Payne corrected values given in our work. For SiC defects, the transition levels involving the same charge states behave similarly but differ by only 0.2 eV. Along the same lines, $0/-1$ and $+1/0$ charge transition levels are estimated to be subject to residual inaccuracies of 0.07 and 0.17 eV for defects in SiC and in SiO_2, respectively.

In this paper, the defect levels are studied through their charge transition levels. These levels correspond to specific values of the electron chemical potential for which two charge states have equal formation energies. Unlike the formation energies, the location of the charge transition levels does not depend on the chemical potentials of the involved atomic species. This is particularly advantageous, especially when the chemical potentials can not be well determined, as this might be the case during a complex process as the thermal oxidation of SiC. We focus on transitions between thermodynamic ground states of different charge states of the defect. These levels correspond to the defect levels that are detected in capacitance-voltage measurements and can thus directly be compared to measured interfacial defect densities. Based on careful comparisons between calculated and measured charge transition levels,[86,87] it is fair to expect that defect levels determined through hybrid functionals deviate from experiment by not more than ~0.2 eV when the band gap is well reproduced. At variance, in photon-stimulated tunneling experiments,[21,22] different defect levels are probed since the atomic structure does not have time to relax to its ground state upon the optical excitation. The transition levels pertaining to such experiments are referred to as vertical transition levels and differ from charge transitions levels by the involved relaxation energies.

In an amorphous environment as that of SiO_2, the determination of charge transition levels may significantly be affected by the structural disorder leading to a spread of the formation energies.[88–91] In this respect, we note that the targeted defects at the origin of the high defect density just below the conduction appear to give rise to a narrow peak, thus suggesting that their atomic structure is reproducibly defined. This argument can thus be used to reject defect models showing large structural reorganizations and large spreads of energy levels. An additional complication concerning the determination of defect formation energies in an amorphous environment is associated with the fact that it is difficult to distinguish defect-induced relaxations from lattice relaxations.[92] The lattice relaxation effects are nevertheless expected to be largely independent of charge state and would thus affect the charge transition levels only marginally. To monitor the role of lattice relaxations, we systematically controlled the recovery of the original structures upon consideration of the inverse charge transition.[92]

E. Interface-specific polarization effects

An obvious limitation of the adopted description is its incapability of describing the polarization conditions at the interface. The extra energy contribution due to the dielectric discontinuity at the interface can be estimated through a simple classical electrostatics model. We consider a system of two adjacent semi-infinite dielectrics with dielectric constants $\epsilon_{\rm SiC}$ and $\epsilon_{\rm SiO_2}$. For instance, a point charge q is embedded in the semi-infinite SiC substrate at a distance d from the interface. Using the image method, an image charge q' symmetric to q with respect to the interface plane is responsible for a potential V given by

$$V = \frac{1}{\epsilon_{\rm SiC}}\frac{q'}{2d} \quad \text{with} \quad q' = -\left(\frac{\epsilon_{\rm SiO_2}-\epsilon_{\rm SiC}}{\epsilon_{\rm SiO_2}+\epsilon_{\rm SiC}}\right) q\,. \tag{2}$$

Finally, the electrostatic energy ΔE due to the charge q at a distance d from the interface is given by $\Delta E = \frac{1}{2} qV$. When q is placed in SiO_2, the same equation applies provided the dielectric constants are exchanged.

Figure 2 shows the electrostatic energy ΔE as a function of the distance of the charge from the interface. The curve is interrupted at a distance of 2 Å because of the artificial divergences occurring in classical electrostatics. The cutoff of 2 Å roughly corresponds to the involved bond lengths, which have been shown to determine the typical length scale required for recovering the bulk susceptibility at interfaces.[93,94] Due to the higher dielectric constant of SiC, the image charge interaction for a charge q placed in the substrate is only a fraction ($\epsilon_{\rm SiO_2}/\epsilon_{\rm SiC} \sim 1/2.4$) of that for q placed in the oxide. It should also be noted that the value of the image charge interaction scales as q^2, which makes it particularly important when the defect is doubly charged.

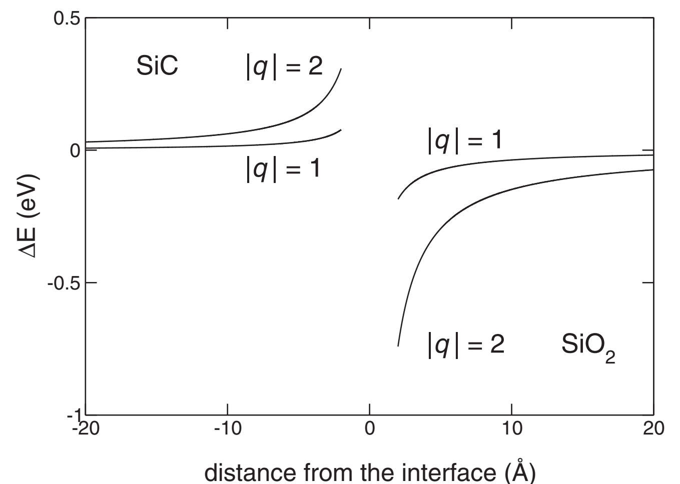

FIG. 2. Polarization corrections to the defect formation energies due to the SiC/SiO_2 interface, as obtained from classical electrostatics.

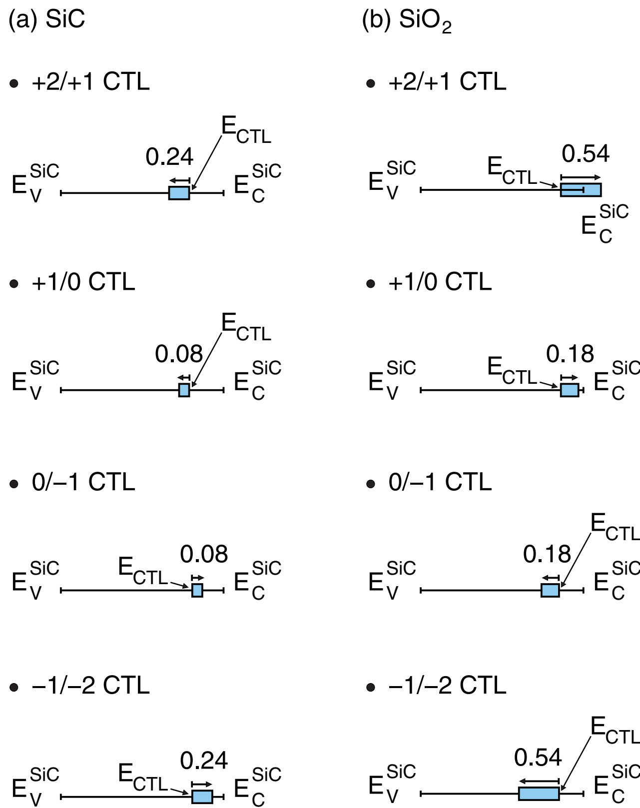

FIG. 3. (Color online) Schematics of the energy range spanned by $+2/+1$, $+1/0$, $0/-1$, and $-1/-2$ charge transition levels (CTLs) at the SiC/SiO_2 interface as obtained through electrostatics corrections for defects located (a) in SiC and (b) in SiO_2. The highlighted energy range corresponds to defects located at distances larger than 2 Å from the interface (see text).

To illustrate the size of this polarization correction, we show in Fig. 3 the range of energies over which the charge transition level may vary depending on the distance of the defect to the interfacial plane. We explicitly consider the cases of $+2/+1$, $+1/0$, $0/-1$, and $-1/-2$ charge transition levels for defects located on both the substrate and oxide sides of the interface. Similar corrections can be found for other charge transitions. All charge transition levels calculated in the following sections are subject to these corrections, which depend on the location of the defect with respect to the interfacial plane.

It should also be mentioned that our approach does not capture any structural relaxation that is specific to the interface. These effects can be estimated by creating the defects directly in the interface model and by monitoring the differences with respect to the corresponding bulk defects through the Kohn-Sham levels.[53] Such relaxation effects appear to be minor. Indeed, the properties of substrate defects are preserved due to the rigidity of the crystalline network, while the high flexibility of the oxide network ensures that oxide defects are only marginally affected by the proximity of the substrate.[53] The difference between structural relaxations in bulk and interfacial systems is thus neglected in the following.

III. CARBON-RELATED DEFECTS

Carbon-related defects have been the object of several previous investigations in which their defect levels were determined through Kohn-Sham levels.[50–53,95] While such studies are useful for providing an understanding of the available defect levels, it has been found that significant quantitative differences might occur with respect to a description based on charge transition levels.[51,53] Therefore, we here reconsider the energy levels of such carbon-related defects on both the substrate and oxide sides of the SiC/SiO_2 interface. A detailed comparison between Kohn-Sham energy levels and charge transition levels is given in the Appendix.

A. Excess carbon in SiC

We start the investigation of excess carbon in SiC by considering in detail the case of the single-carbon interstitial. This defect gives rise to a C-C pair defect situated at a C site in bulk 4*H*-SiC, as illustrated in Fig. 4. In this defect configuration, the carbon atoms of the C-C pair only have Si neighbors. In bulk SiC, there are two variants of this defect corresponding to two inequivalent C sites. These C sites differ by the distance $d_{\text{C}-\text{Si}_\text{b}}$ between the unperturbed C atom occupying the site and a nearby Si atom belonging to the next bilayer, as shown in Fig. 5. The considered pair defect models are labeled in the following as $(\text{C-C})_{\text{SiC}}$ for $d_{\text{C}-\text{Si}_\text{b}} = 3.17$ Å and $(\text{C-C})'_{\text{SiC}}$ for $d_{\text{C}-\text{Si}_\text{b}} = 3.63$ Å.

Upon charging, the defect structure undergoes significant modifications. When one electron is introduced in the $(\text{C-C})_{\text{SiC}}$ configuration, one carbon atom of the C-C pair binds to a neighboring silicon atom, which thus becomes fivefold coordinated [Fig. 6(a)]. It should be noted that this fivefold-coordinated Si atom is not a neighboring atom of the C-C pair defect in the neutral $(\text{C-C})_{\text{SiC}}$ configuration. This bonding arises due to the relatively small distance $d_{\text{C}-\text{Si}_\text{b}} = 3.17$ Å between the C lattice site and a Si atom of the next bilayer in the $(\text{C-C})_{\text{SiC}}$ configuration (cf. Fig. 5). In the $(\text{C-C})'_{\text{SiC}}$ configuration, the larger distance $d_{\text{C}-\text{Si}_\text{b}} = 3.63$ Å prevents this bonding, and the introduction of a negative charge results in two first-neighbor Si atoms of the C-C pair becoming fivefold coordinated [Fig. 6(b)]. These fivefold-coordinated Si atoms belong to two adjacent Si-C bilayers. Upon the introduction of a second electron, the $(\text{C-C})_{\text{SiC}}$ and $(\text{C-C})'_{\text{SiC}}$ structures undergo only minor changes. The main structural parameters are summarized in Table I.

The formation energies of the negative (-1) charge state of the $(\text{C-C})_{\text{SiC}}$ pair defect versus electron chemical potential in

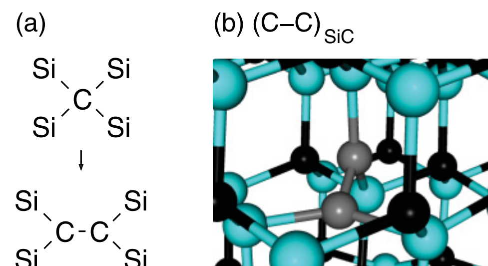

FIG. 4. (Color online) (a) Schematics and (b) ball-and-stick representation of the C-C pair defect in bulk SiC.

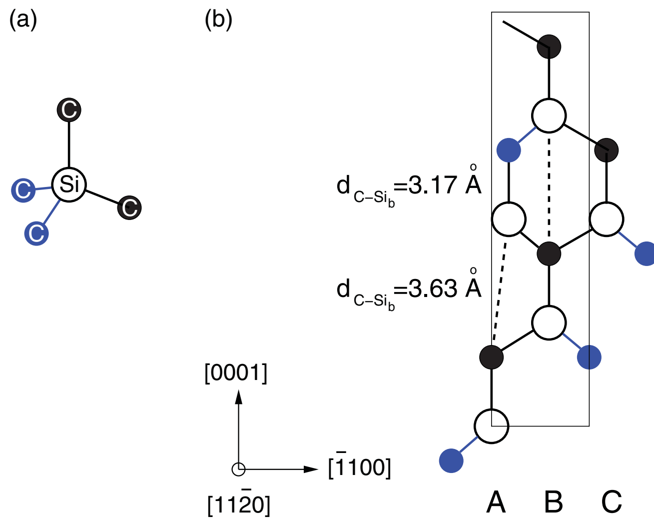

FIG. 5. (Color online) (a) Schematics of the basic structural unit of SiC consisting of a tetrahedron of four carbon atoms with a silicon atom at its center. Si and C atoms are represented by open and filled balls, respectively. The dark C atoms are located in the plane of the paper. (b) Projection of the stacking sequence of Si and C bilayers in 4H-SiC/SiO$_2$ on the (11$\bar{2}$0) plane. The two shortest distances (dotted lines) between a C atom and a Si atom of the next bilayer identify two different C sites.

bulk 4H-SiC are shown at the PBE and PBE(0.15) levels of theory in Fig. 7. The position of the charge transition level $E^{0/-1}$ is defined as the value of the chemical potential at which the neutral and singly negative charge states of the C-C pair defect have equal formation energies. $E^{0/-1}$ in PBE and PBE(0.15) calculations differ considerably when referred to the conduction band. It locates at $E_c-0.36$ eV and $E_c-0.73$ eV at the PBE and PBE(0.15) levels of theory, respectively. However, when referred to the electrostatic potential, $E^{0/-1}$ determined with the two functionals agrees very well, in accord with the general behavior of atomically localized defects.[69,70,96,97]

A similar agreement between PBE and PBE(0.15) is found for $E^{+2/+1}$ and $E^{+1/0}$ as shown in Fig. 8. At the PBE level, the $E^{-1/-2}$ level falls above the conduction band after the Makov-Payne correction is applied.[82] However, the defect in the charge state $q=-2$ can be relaxed and gives a localized defect wave function. When the band gap is opened at the PBE(0.15) level,

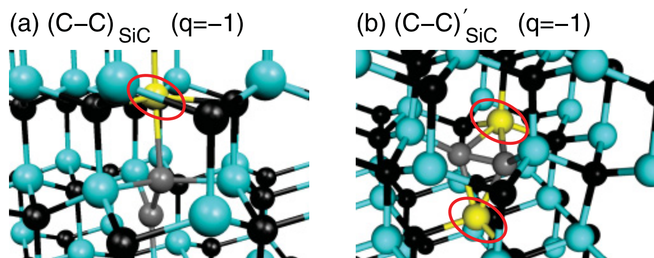

FIG. 6. (Color online) The C-C pair defect in bulk 4H-SiC. The (a) (C-C)$_{SiC}$ and (b) (C-C)$'_{SiC}$ models are shown in the charge state $q=-1$. Overcoordinated Si atoms resulting from defect charging are highlighted in yellow and circled by ellipses.

TABLE I. Distance and angle parameters of the C-C defect structures in bulk SiC and bulk SiO$_2$, in the neutral and negative charge states. Charges (q) are given in atomic units and distances in Å. Si* refers to the silicon atom fivefold (sixfold) coordinated to one (two) of the carbon atoms of the C-C pair. The two Si*-C distances are averaged in the doubly negatively charged (C-C)$_{SiO_2}$ structure. The values in parentheses indicate standard deviations.

	q	C-C	Si-C	Si*-C	∠ Si-C-Si	∠(sp^2 pl.)
(C-C)$_{SiC}$	0	1.37	1.79		138.4° (1.3°)	89.3°
(C-C)$_{SiC}$	−1	1.43	1.79	2.08	135.0° (2.6°)	
(C-C)$_{SiC}$	−2	1.48	1.81	1.96	132.1° (16.2°)	
(C-C)$'_{SiC}$	0	1.35	1.79		137.4° (0.7°)	84.2°
(C-C)$'_{SiC}$	−1	1.41	1.84	1.92	128.1° (3.7°)	
(C-C)$'_{SiC}$	−2	1.47	1.83	1.91	127.0° (0.7°)	
(C-C)$_{SiO_2}$	0	1.37	1.86		124.0° (13.6°)	6.4°
(C-C)$_{SiO_2}$	−1	1.51	1.86	1.95	117.8° (7.8°)	
(C-C)$_{SiO_2}$	−2	1.62	1.81	1.96	120.8° (14.1°)	
(C-C)$'_{SiO_2}$	0	1.46	1.91		94.6° (5.8°)	80.4°
(C-C)$'_{SiO_2}$	−1	1.50	1.85		95.4° (5.1°)	73.6°
(C-C)$'_{SiO_2}$	−2	1.57	1.80		96.8° (4.5°)	78.1°

the $E^{-1/-2}$ level falls well within the SiC band gap.[98] We note that the charge transition levels involving high charge states ($|q|=2$) are possibly subject to the largest inaccuracies due to the Makov-Payne[82] overcorrection effect (see Sec. II D). For instance, the application of the Lany-Zunger correction scheme[83] would lead to $+2/+1$ ($-1/-2$) levels, which are higher (lower) by 0.2 eV.

To estimate the energy range spanned by the charge transition levels at the SiC/SiO$_2$ interface, it is necessary to include the interface-specific electrostatics corrections discussed in Sec. II E. The calculated charge transition levels

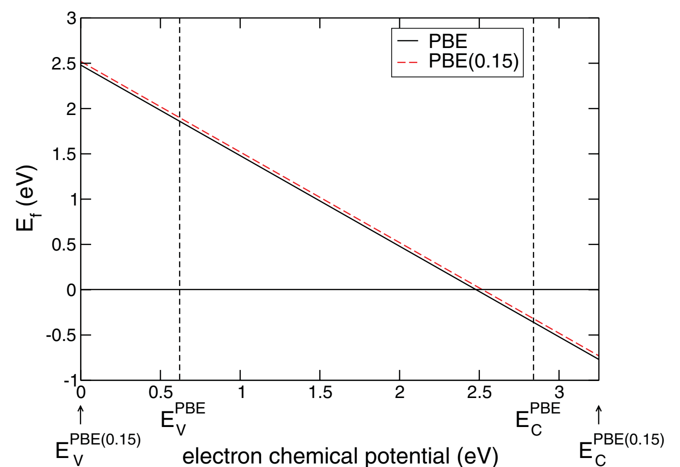

FIG. 7. (Color online) Formation energies of the −1 charge state of the (C-C)$_{SiC}$ defect vs electron chemical potential in bulk 4H-SiC at the PBE (solid black) and PBE(0.15) (dashed red) levels of theory. The formation energies are referred to that of the neutral defect. The valence band of bulk 4H-SiC in the PBE(0.15) calculation is used as the reference for the electron chemical potential. The valence- and conduction-band edges at the PBE level are positioned with respect to those at the PBE(0.15) level through the alignment of the average electrostatic potential.

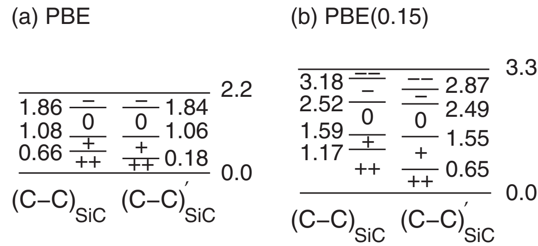

FIG. 8. Charge transition levels (CTLs) of the C-C pair defect in bulk 4H-SiC in a schematics of the SiC band gap. The CTLs are calculated at the (a) PBE and (b) PBE(0.15) levels. The two calculations are aligned through the average electrostatic potential of the unperturbed bulk. The energies are referred to the SiC valence band. Energies are given in eV. Interface-specific electrostatics corrections are not included.

are first positioned with respect to the SiC band edges, as in Fig. 8. The electrostatics correction depends on distance to the interface. To consider a representative range, we take a minimal distance of $d = 2$ Å (cf. Sec. II E). This determines the energy range over which the charge transition level varies. For defects located on the SiC side of the interface, the correction shifts the $+2/+1$ and $+1/0$ charge transition levels downward and the $0/-1$ and $-1/-2$ charge transition levels upward (Fig. 3). For instance, considering the two defect configurations, we find that the $0/-1$ charge transition level at the interface is expected to locate between $E_C^{SiC}-0.8$ eV and $E_C^{SiC}-0.7$ eV, where E_C^{SiC} is the energy of the SiC conduction band, while the $-1/-2$ charge transition level extends from $E_C^{SiC}-0.4$ eV to $E_C^{SiC}+0.2$ eV. The energy ranges spanned by the other defect levels can be determined in a similar way.

The C-C defect on the SiC side of the interface shows energy levels spanning the whole band gap of SiC. In particular, it also presents defect levels lying close to the conduction band. However, the characteristics of this defect do not match the properties of the experimentally observed peak of NITs since this peak does not present any correlation with defect levels in the lower part of the SiC band gap. We therefore conclude that it is unlikely that C-C pairs in SiC are at the origin of the NITs observed just below the SiC conduction band. This conclusion confirms previous considerations based on Kohn-Sham energy levels.[50,53]

Carbon interstitials in SiC are expected to be highly mobile,[99] and the energetics for aggregation is particularly favorable.[100] We therefore also considered the double-carbon interstitial in SiC.[57] Following the same scheme, we found four charge transition levels for this defect in the SiC band gap: $+2/+1$, $+1/0$, $0/-1$, and $-1/-2$, at 0.49, 0.71, 3.02, and 3.21 eV from the valence-band maximum, respectively.[57] Given the number and the distribution of the energy levels of this defect, the same considerations apply as for the single interstitial, ruling the double interstitial carbon out as origin for the high defect density near the conduction-band edge. Nevertheless, following an alternative reasoning, a recent study has identified this defect as the main origin for the poor mobilities at SiC/SiO_2 interfaces.[99]

We here do not extend our study to consider aggregation states involving a higher number of carbon atoms. Indeed, the tendency observed for the single and double interstitials suggests that such aggregates would give rise to numerous defect levels distributed quite uniformly throughout the SiC band gap, in agreement with expectations based on general considerations.[4] Hence, such defects are expected to contribute to the background defect density, but their distribution in the band gap is inconsistent with the high defect density found in the vicinity of the conduction-band edge of SiC.

B. C-C pair defect in SiO_2

We also considered excess carbon in the form of a C-C pair defect located in the amorphous SiO_2 on the opposite side of the interface.[51,53] Several models can be designed, which mainly differ by the dihedral angle between the two planes defined by the threefold-coordinated C atoms and by the nature of the first neighbors.[53] The C-C pair defect with Si neighbors is expected to give defect levels falling close to the conduction band, while C-C pairs with carbon or oxygen neighbors give higher-lying levels.[53] We here thus consider two configurations with Si nearest neighbors, as illustrated in Fig. 9. These two configurations are referred to as $(C\text{-}C)_{SiO_2}$, and $(C\text{-}C)'_{SiO_2}$ and mainly differ by the involved dihedral angles (cf. Table I).

Upon charging, different scenarios occur. When a spectator Si atom is found nearby the C-C defect as for the $(C\text{-}C)_{SiO_2}$ structure, this Si atom becomes fivefold coordinated upon addition of one electron [Fig. 10(a)], in a similar way as observed on the SiC side of the interface. Upon introduction of a second electron, the fivefold-coordinated Si atom bonds to the second carbon atom of the $(C\text{-}C)_{SiO_2}$ pair and becomes sixfold coordinated [Fig. 10(b)]. At variance, there are no nearby Si atoms in the $(C\text{-}C)'_{SiO_2}$ configuration [Fig. 10(c)] and the structure hardly changes upon charging. To ensure that the charge transition levels are not affected by lattice relaxations of the amorphous network, we checked that the configurations in Fig. 10 return to their stable neutral configurations upon decharging.[92]

In Fig. 11, the charge transition levels of the two defect configurations are positioned within the band diagram of the SiC/SiO_2 interface, as obtained at both the PBE and PBE(0.35) levels of theory. When the two calculations are aligned through the electrostatic potential, corresponding charge transition levels are again found to lie very close.[69,70,96,97] The charge transition levels obtained within the hybrid functional scheme can directly be compared with experiment as the description of the band gaps and the band offsets are well reproduced.[86,87]

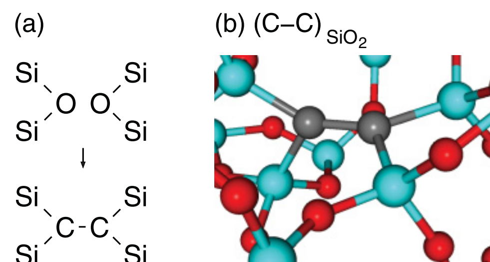

FIG. 9. (Color online) (a) Schematics and (b) ball-and-stick representation of the C-C pair defect in bulk SiO_2.

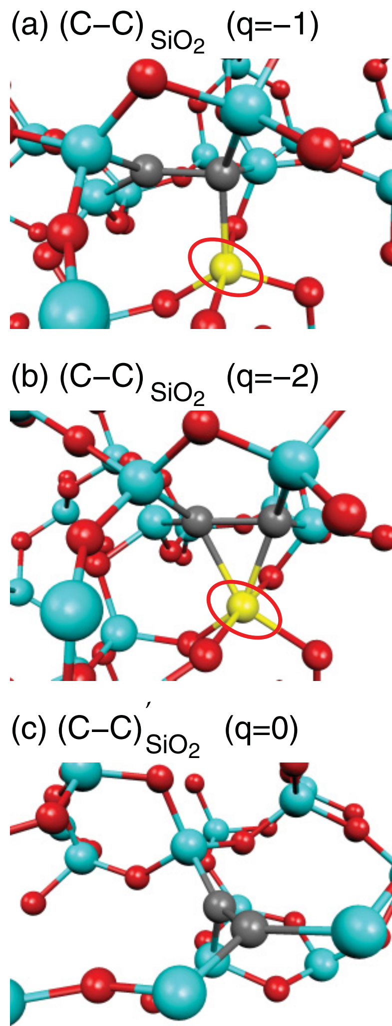

FIG. 10. (Color online) The C-C pair defect in bulk SiO_2. The $(C\text{-}C)_{SiO_2}$ model is shown in the charge states (a) $q = -1$ and (b) $q = -2$, and the $(C\text{-}C)'_{SiO_2}$ is shown in the (c) neutral state ($q = 0$). Overcoordinated Si atoms resulting from defect charging are highlighted in yellow and circled by ellipses.

In the following, we will therefore focus the discussion only on the results achieved with hybrid functionals.

Because of the varying structural environment in the amorphous oxide, the charge transition levels of the considered defect configurations are noticeably different. However, both configurations show defect levels just below the conduction band and in the proximity of the valence band. Due to Makov-Payne overcorrection, the $+2/+1$ $(-1/-2)$ charge transition levels are subject to the largest inaccuracies and might shift upward (downward) by up to 0.5 eV (see Sec. II D). Interfacial electrostatics effects lower the $0/-1$ charge transition level by ~0.2 eV, but increase the $0/+1$, $+1/+2$, and $0/+2$ ones by ~0.2, ~0.5, and ~0.7 eV, respectively. The defect levels lying close to the SiC valence band might escape detection, but those lying close to the conduction band can be found as low as at $E_C^{SiC}-0.7$ eV. Our work thus leads to defect levels, which are in substantial agreement with those previously found by Knaup *et al.*[51] However, we reach a different conclusion about these defects as a possible origin of the observed NITs.

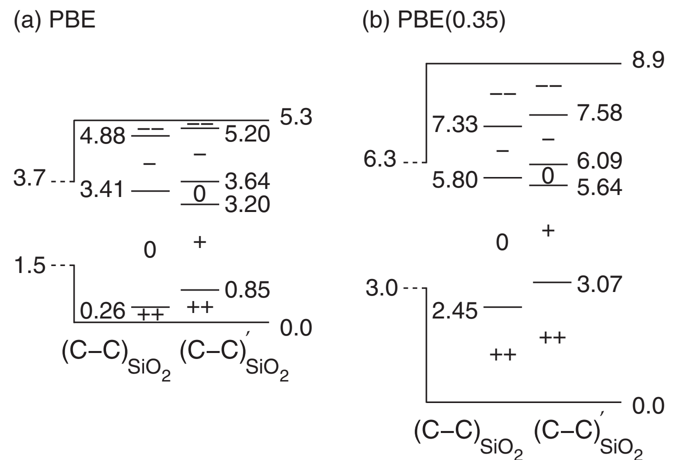

FIG. 11. Charge transition levels (CTLs) of the C-C pair defects in bulk SiO_2 in a band diagram of the SiC/SiO_2 interface. The CTLs are calculated (a) at the PBE and (b) at the PBE(0.35) levels. The two calculations are aligned through the average electrostatic potential of the unperturbed bulk. The energies are given in eV and are referred to the valence-band edge of SiO_2. The method presented in Sec. II C is used for determining the band offset. Interface-specific electrostatics corrections are not included.

According to the analysis in Ref. 53, C-C defects in amorphous SiO_2 with other nearest neighbors are expected to give defect levels lying even higher in the SiC band gap. This analysis thus suggests that the charge transition levels associated to C-C defects in SiO_2 finally span a broad energy range around the SiC conduction band, which is expected to contribute in some form to the density of defect states in the upper part of the SiC band gap. However, the properties of this defect appear unlikely to give rise to a narrow feature in the defect density near the conduction-band edge, as observed for the NITs.

C. Single-carbon atoms in SiO_2

Two defect structures involving single-carbon atoms in the oxide are studied here. We first consider a carbon atom replacing a silicon atom and thus forming a bond to four oxygen atoms, labeled as $C\text{-}O_4$ in the following. Then, we study a CO unit replacing an oxygen atom of a Si-O-Si linkage and thus forming a $Si_2\text{-}C\text{-}O$ structure in three different configurations, labeled as $(Si_2\text{-}C\text{-}O)_n$, where n is the configuration number. The latter defect has previously been identified as a metastable defect occurring during SiC oxidation.[101] Schematics and ball-and-stick representations for these two defects are shown in Figs. 12 and 13, respectively.

When one carbon atom replaces one silicon atom in the oxide network, the structural rearrangement is driven by the shorter C-O distance. In the relaxed structure, the average C-O bond length is 1.40 Å, about 16% shorter than the average Si-O bond length in the oxide. All the other structural parameters remain almost unchanged upon replacement of a silicon atom by a carbon atom, even upon charging. The chemical similarity of carbon and silicon is also noticeable in the positions of the charge transition levels of the $C\text{-}O_4$ defect model, as shown in Fig. 14. The $+1/0$ and the $0/-1$ charge transition levels are located in the close vicinity of the SiO_2 conduction and

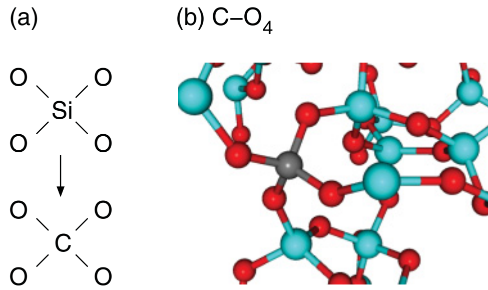

FIG. 12. (Color online) (a) Schematics and (b) ball-and-stick representation of the C-O_4 structure. The inserted carbon atom is gray (dark).

valence bands, respectively. The C-O_4 defect model does not give rise to any defect level in the SiC band gap.

In the three models of the Si_2-C-O structure, the carbon atom is threefold coordinated in the neutral charge state [cf. Fig. 13(b)]. The average Si-C bond length of 1.89 Å is comparable to the bond length in the SiC substrate, and the average C-O bond length is 1.24 Å. The Si-C-O angles are about 115°. The three angles on the C atom sum up to 357.7° on average, indicating that the defect structure is very close to planar. Different scenarios take place upon charging (cf. Fig. 15). Either one [Figs. 15(a), 15(b), and 15(d)] or two [Fig. 15(c)] of the neighboring Si atoms can become fivefold coordinated. The carbon atom can remain threefold coordinated [Figs. 15(b) and 15(d)] or become fourfold coordinated [Figs. 15(a) and 15(c)].

However, these differences in structural configurations do not have a major impact on the overall location of the charge transition levels (Fig. 16). In the three configurations, the $+1/0$ charge transition level extends from E_V^{SiC} to $E_V^{SiC}+0.4$ eV, where E_V^{SiC} corresponds to the valence-band edge of SiC, while the $0/-1$ charge transition level locates between $E_C^{SiC}+0.1$ eV to $E_C^{SiC}+0.4$ eV. The $-1/-2$ charge transition level is less localized but is found well above the conduction band of SiC, and this result is not affected by the possible overestimation of the Makov-Payne correction (see Sec. II D). Consideration of the interfacial electrostatics effects discussed in Sec. II E leads to a lowering of the $0/-1$ charge transition levels over an energy range spanning ~0.2 eV, while the $+1/0$ level would shift over a comparable range in the opposite direction. The $0/-1$ charge transition level of a Si_2-C-O defect close to the interface would then locate just below the SiC conduction band, while its $+1/0$ charge transition level would fall near

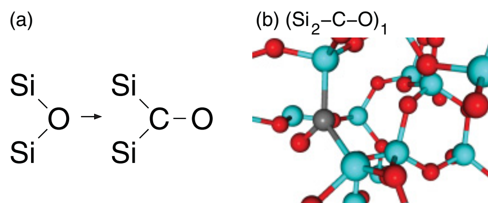

FIG. 13. (Color online) (a) Schematics and (b) ball-and-stick representation of the Si_2-C-O structure. The inserted carbon atom is gray (dark) and is threefold coordinated, while its neighboring O atom is nonbonding. The $(Si_2\text{-C-O})_1$ structure is represented in its neutral charge state.

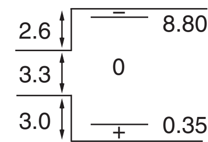

FIG. 14. Charge transition levels of the C-O_4 defect at the PBE(0.35) level in a schematics of the band-gap evolution across the SiC/SiO_2 interface. Energies are given in eV. Interface-specific electrostatics corrections are not included.

to the valence-band edge of SiC. Within the intrinsic errors of our approach, the Si_2-C-O defect could therefore present an electron trap level near the conduction band edge of SiC, while its associated donor state could remain undetected due to its proximity to the valence band. The defect levels of the Si_2-C-O structure might therefore be consistent with the distribution of NIT levels measured experimentally at the SiC/SiO_2 interface. The assignment of the Si_2-C-O structure to the observed traps is also consistent with the observed correlation of the latter defects with the availability of carbon at the interface.[102] Also, it appears straightforward to picture the effect of passivation by nitridation, in which the nitrogen atom could replace the carbon atom preserving the local threefold coordination.

On the other hand, this assignment can not trivially be reconciled with the observation that the defects at the origin of the NITs at SiC/SiO_2 interfaces would occur in similar concentrations at Si/SiO_2 interfaces.[21,22] However, the latter observation relies on photon-stimulated tunneling experiments detecting vertical transition levels, and it is not clear whether the involved defects correspond to the same NIT defects measured in capacitance-voltage experiments. To illustrate this difference, we calculate vertical transitions associated to the three Si_2-C-O defects studied in this work. To reproduce the

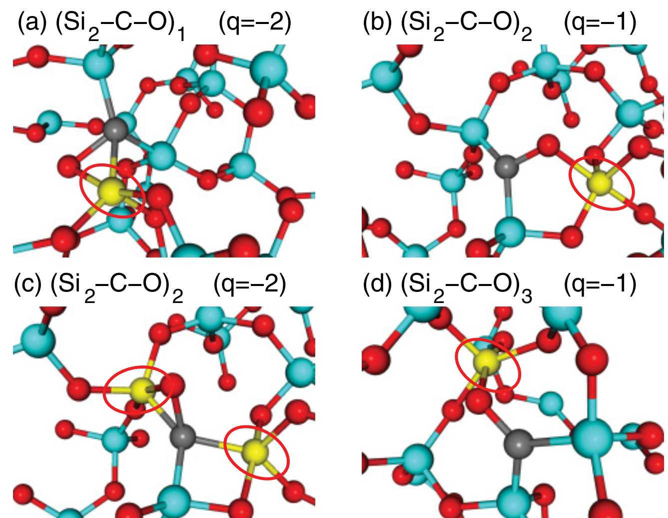

FIG. 15. (Color online) Ball-and-stick representations of the Si_2-C-O structure in different configurations and charge states. (a) The first configuration is represented in the doubly negative charge state $q=-2$, the second configuration in the charge states (b) $q=-1$ and (c) $q=-2$, and (d) the third configuration in the charge state $q=-1$. The fivefold coordinated Si atoms are highlighted in yellow are circled by ellipses.

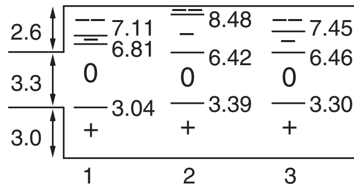

FIG. 16. Charge transition levels for the three models of the Si_2-C-O structure in a schematics of the band-gap evolution across the SiC/SiO_2 interface, as obtained at the PBE(0.35) level. Energies are given in eV. Interface-specific electrostatics corrections are not included.

experimental conditions,[21,22] we consider the $-1 \rightarrow 0$ charge transition without allowing the structure to relax in the final state. The corresponding vertical charge transition levels are found at 6.08, 5.04, and 4.44 eV from the SiO_2 valence band.[103] We note that these levels are located well within the band gap of SiC and are broadly distributed, in strong contrast with the thermodynamic $0/-1$ charge transition levels calculated for the same structures (Fig. 16).

IV. OXYGEN-RELATED DEFECTS

Intrinsic defects in SiO_2 have been proposed to account for the D_{it} in the upper band gap of SiC.[6,20–23] We here consider a series of such defects associated to oxygen deficiency and oxygen excess, respectively.

A. Oxygen-deficiency defects

The transition layer at the SiC/SiO_2 interface has been shown to contain partially oxidized silicon atoms[104] consisting of oxygen-deficient centers such as oxygen vacancies. Oxygen vacancies in amorphous SiO_2 may give rise to a large variety of defect configurations.[89] However, the only one that may give rise to a well-defined and reproducible local atomic structure is the Si-Si dimer bond (Fig. 17). We generated such a defect by extracting an O atom from our bulk model of SiO_2 and allowing for structural relaxation. In the neutral charge state, we find a bond distance of 2.47 Å, only slightly larger than for a Si-Si bond in an isolated cluster (2.35 Å) (Ref. 105) and close to results for α-quartz [2.45 Å (Ref. 106) and 2.4 Å (Ref. 107)]. This suggests that the structural model for the Si-Si bond adopted in this work is a valid representative of a typical situation.

We also consider this defect in the positive and negative charge states, and calculate charge transition levels as de-

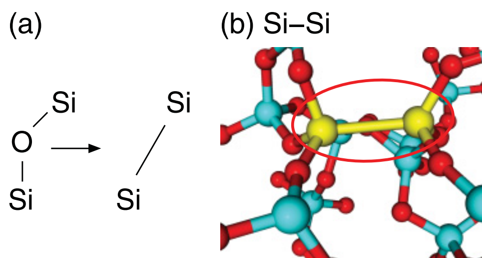

FIG. 17. (Color online) (a) Schematics and (b) ball-and-stick representation of the Si-Si bond defect. The Si atoms forming the Si-Si bond are highlighted in yellow and circled by an ellipse.

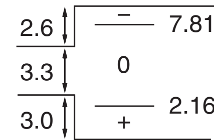

FIG. 18. Charge transition levels of the Si-Si bond defect calculated at the PBE(0.35) level in a schematics of the band-gap evolution across the SiC/SiO_2 interface model. Energies are given in eV. Interface-specific electrostatics corrections are not included.

scribed in Sec. II D. The relaxations of the defect structures lead to Si-Si bond lengths of 3.36 and 3.86 Å in the positive and negative charge states, respectively. Otherwise, the bonding arrangement remains the same throughout the different charge states. The positions of the charge transition levels are schematically represented in Fig. 18. The $+1/0$ charge transition level occurs 0.8 eV below the SiC valence band, in good agreement with previous results,[106,108] while the $0/-1$ charge transition level occurs 1.5 eV above the SiC conduction band. Both charge transition levels are therefore far from the SiC band gap. To have this defect contribute to the defect density in the band gap, considerable broadening needs to be invoked because of structural disorder.[89] Hence, the Si-Si bond defect is not expected to be at the origin of the narrow peak occurring close to the conduction-band edge of SiC.

Another variant of the O vacancy in SiO_2 is the Si dangling-bond defect, in which the Si atoms facing the vacancy undergo asymmetric relaxations.[109] In α-quartz, this defect is known as E_1' and has been the object of numerous theoretical studies.[106,107,109–111] In a study using the same methodology as applied in this work, the $+1/0$ charge transition level was found at 5.6 eV from the valence-band edge of SiO_2, i.e., within the SiC band gap at 0.6 eV from the conduction band.[108] This location is in qualitative agreement with a calculation at the semilocal level, which found the defect level in the middle of the Si band gap.[106] Electrostatics corrections for defects lying close to the interface shift this level to higher energies, up to about 0.2 eV. While a systematic study of the charge transition levels of the corresponding E_γ' defect in amorphous SiO_2 is to our knowledge not yet available, this defect is not expected to give rise to a narrow peak in the defect density. Indeed, the stabilizing agent of E_γ' is a suitably located O atom, which becomes threefold coordinated upon positive charging,[106,107,109–111] thereby making the formation of this defect highly dependent on the local environment.[89,111] Thus, the E_γ' defect can not plausibly be invoked as a possible origin of the observed NITs. This conclusion supports previous considerations on the role of E_γ'.[51]

The silicon interstitial was studied by Knaup *et al.* as a possible candidate among the oxygen-deficiency defects.[51] Careful inspection of their model structure reveals that this defect configuration corresponds to a Si atom in the partial oxidation state +2. In other terms, this defect can be pictured as two nearby oxygen vacancies giving rise to a chain of 3 Si atoms connected by Si-Si bonds. Knaup *et al.* studied one configuration of this kind. A $0/-1$ charge transition level was found at 6.83 eV from the valence band of SiO_2, only slightly higher than the conduction-band edge of SiC, while a $+1/0$

charge transition level occurred well below the valence-band edge of SiC at 2.49 eV from the valence band of SiO_2.[51] On the basis of these results, Knaup *et al.* could therefore propose the silicon interstitial as a possible origin of the NITs.[51] To further examine this possibility, we also generate two different defect structures of this kind, showing Si-Si-Si chains in our 144-atom model of SiO_2. For one of these defects, we calculate $+1/0$ and $0/-1$ charge transition levels at 3.67 and 7.69 eV, respectively, while for the other we obtain respective levels at 4.07 and 7.60 eV. In our approach, both levels are located at higher energies with respect to results of Knaup *et al.*[51] The $0/-1$ levels are found well above the conduction-band edge of SiC, while the $+1/0$ levels now occur in the lower part of the band gap of SiC. According to these results, this kind of defect structure no longer appears as a viable candidate for the high defect density of the NITs. Furthermore, given the extended nature of this defect with a core involving three Si atoms, we expect its energy levels to be particularly sensitive to the environment and to give rise to a broad distribution of levels in the defect density.

B. Excess oxygen defects

We then investigate excess oxygen defects resulting from the oxidation of SiC. For instance, a single oxygen atom could incorporate a Si-C bond of the SiC substrate [Fig. 19(a)]. As another possibility, a carbon atom of the SiC substrate could be replaced by the two oxygen atoms of an incoming O_2 molecule, giving rise to two regular Si-O-Si linkages [Fig. 19(b)]. An additional oxygen atom could also incorporate in a Si-O-Si bond, thereby forming a Si-O-O-Si bridge (peroxy linkage) [Fig. 19(c)].

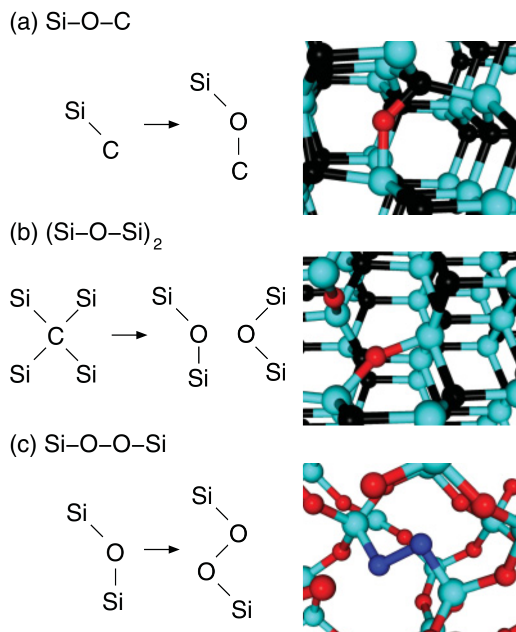

FIG. 19. (Color online) Schematics and ball-and-stick representations of three excess oxygen-related defects modeled in (a), (b) bulk SiC and (c) α-quartz (cf. text for details). The oxygen atoms of the Si-O-O-Si bridge are represented by dark balls (in dark blue).

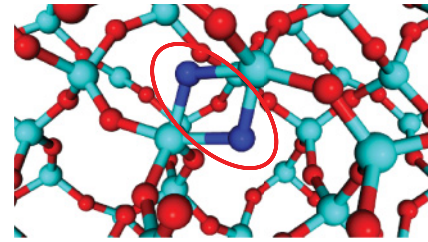

FIG. 20. (Color online) The Si-O-O-Si bridge defect in α-quartz is shown in the charge state $q=-1$. The oxygen atoms of the Si-O-O-Si bridge are highlighted in dark blue and circled by an ellipse.

The Si-O-C and $(Si\text{-}O\text{-}Si)_2$ structures are modeled in bulk SiC. In the neutral charge state, these structures feature small structural relaxations of the defect environment compared to the defect-free structures. For example, the single interstitial oxygen atom in a Si-C bond [Fig. 19(a)] buckles out of a Si-C bilayer and has regular Si-O and C-O bond lengths of 1.61 and 1.42 Å, respectively. The replacement of one carbon atom by two O atoms leads to a structure [Fig. 19(b)] presenting an average Si-O bond length of 1.64 Å and an average Si-O-Si angle of 161.8°, which are typical values for amorphous SiO_2. Upon charging, the structural relaxations in the Si-O-C and $(Si\text{-}O\text{-}Si)_2$ structures are minor due to the stiffness of SiC and the bonding arrangement remains unaffected. Moreover, no charge transition levels are found in the SiC band gap, which discards these two defect structures as candidates for the high D_{it} near the SiC conduction band.

The Si-O-O-Si bridge defect has been the object of numerous theoretical studies.[112–116] To model this bridge defect, we first use the α-quartz structure of SiO_2. This crystalline structure accounts for the stiffness of the oxide at the SiC/SiO_2 interface. In the neutral charge state, the Si-O bonds involved in the Si-O-O-Si bridge feature regular lengths of 1.66 and 1.67 Å. The neighboring Si atoms of the O-O bond are significantly relaxed, increasing the Si-Si distance by 0.6 Å with regard to unperturbed α-quartz. The O-O bond distance is 1.51 Å. In the charge state $q=-1$, the peroxy linkage transforms to a double-bridge structure, as shown in Fig. 20. The double-bridge structure corresponds to the most stable configuration also in the charge state $q=-2$. The relaxed configurations found in our study are in good agreement with those identified in previous investigations of the Si-O-O-Si bridge defect in α-quartz and amorphous SiO_2.[112–116]

The corresponding charge transition levels are shown in a schematics of the band-gap evolution across the interface in Fig. 21. In order to locate the charge transition levels calculated in α-quartz in an energy diagram of the interface model, the electronic structure of α-quartz is aligned to that of amorphous SiO_2 model through the O 2*s* levels.[75]

The charge transition levels related to the peroxy linkage (Si-O-O-Si bridge defect) span the upper half of the SiC band gap. After proper alignment,[75] we find the $0/-1$ and $-1/-2$ charge transition levels at 5.43 and 5.97 eV from the valence-band edge of SiO_2 (Fig. 21). Applying the electrostatics correction scheme of Lany and Zunger[83] rather than that of Makov and Payne,[82] we find that these levels would fall slightly deeper in the band gap, at 5.26 and 5.47 eV, respectively (see Sec. II D). In a previous study at the semilocal

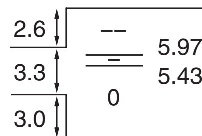

FIG. 21. Charge transition levels of the Si-O-O-Si bridge defect in a schematics of the band-gap evolution across the SiC-SiO_2 interface. The charge transition levels were calculated with the PBE(0.35) functional in α-quartz SiO_2 and incorporated in the band diagram via the alignment of the O 2s states. Energies are given in eV. Interface-specific electrostatics corrections are not included.

level, Stoneham *et al.* found corresponding levels at 3.10 and 3.35 eV,[114] which compare well with our results after correcting for the band-gap underestimation through a shift of the valence band by 2.5 eV.[69,75] Electrostatics correction due to the interface push the levels downward, enlarging the involved energy range further. Hence, on the basis of these results, this defect is not expected to contribute to the high D_{it} near the SiC conduction band. We also modeled the Si-O-O-Si bridge defect in three different configurations in amorphous SiO_2, finding qualitatively similar results as for α-quartz, in accord with a previous study.[114]

As a final consideration concerning excess oxygen defects, we focus on the interstitial O_2 molecule, which plays an important role in the oxidation of SiC and Si. In a previous study,[73,108] this molecule was found to have a $0/-1$ charge transition level at 6.6 eV from the valence-band edge of SiO_2, i.e., at 0.3 eV above the conduction-band edge of 4H-SiC. This calculated level substantially agrees with the value of 7 eV, derived by correcting[69,75] the result of a previous study at the semilocal level.[114] Interface-specific electrostatics corrections would bring this defect level in the close vicinity of the conduction-band edge of 4H-SiC for molecules located close to the interface.[73] Since this interstitial defect does not show any other levels in the SiC band gap, its energy spectrum matches that of the NITs observed in the interface density of states at SiC/SiO_2 interfaces. However, such interstitial O_2 molecules correspond to the most stable form of oxygen in amorphous SiO_2 and are only weakly bound to the oxide network.[65,90] It is therefore expected that they could easily be outgassed by thermal processing.

V. HYDROGEN-RELATED DEFECTS

We here investigate the hydrogen-complexed oxygen vacancy (or hydrogen bridge defect), in which a hydrogen atom is located at an oxygen vacancy and bridges two silicon atoms,[106,117] as shown in Fig. 22. This defect has been proposed in the literature as a possible origin of the NITs.[20,23]

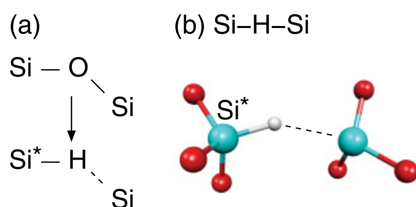

FIG. 22. (Color online) (a) Schematics and (b) ball-and-stick representation of the hydrogen bridge defect. Si* refers to the silicon atom lying closer to the bridging hydrogen atom.

TABLE II. Structural parameters for the hydrogen bridge defect structure averaged over four different configurations for each charge state q. Si* refers to the silicon atom lying closer to the bridging hydrogen. Standard deviations are given in parentheses.

q	-1	0	$+1$
Si*-Si (Å)	3.24 (0.27)	3.18 (0.20)	3.09 (0.20)
Si*-H (Å)	1.51 (0.07)	1.49 (0.02)	1.60 (0.07)
Si-H (Å)	2.34 (0.32)	2.32 (0.09)	1.88 (0.28)
∠ Si*-H-Si	113.2° (7.6°)	119.8° (17.6°)	129.2° (20.6°)

The defect is created in the 72-atom bulk SiO_2 model introduced in Sec. II B. Four different configurations of the hydrogen bridge defect are investigated. For each configuration, the structure is fully relaxed in three charge states (−1, 0, and +1). The averaged structural parameters for the hydrogen bridge defect structure are summarized in Table II. One notices that in the negative and neutral charge states, the position of the hydrogen atom is strongly asymmetric with respect to the two silicon atoms. The Si-H distances differ by ∼35% and the H atom does not fall on the line joining the two Si atoms. When the system accommodates a positive charge, the distances between the hydrogen and the silicon atoms differ much less and the hydrogen atom locates closer to the Si*-Si line. The standard deviations of the angle and the distances show that the hydrogen bridge defect features slightly different configurations, depending on the environment.

We then calculate the charge transition levels as described in Sec. II D. The average $+1/0$ and $0/-1$ charge transition levels calculated at the PBE(0.35) level are located at 4.73 and 6.40 eV above the SiO_2 valence band, respectively. As schematically shown in Fig. 23, the $+1/0$ and $0/-1$ charge transition levels are both located in the upper part of the SiC

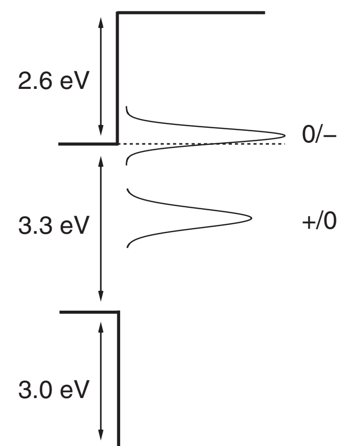

FIG. 23. Charge transition levels of the hydrogen bridge calculated at the PBE(0.35) level in a schematics of the band-gap evolution across the SiC/SiO_2 interface. The levels are schematically illustrated with Gaussian functions with the same standard deviation as the distribution of calculated defect levels. Interface-specific electrostatics corrections are not included.

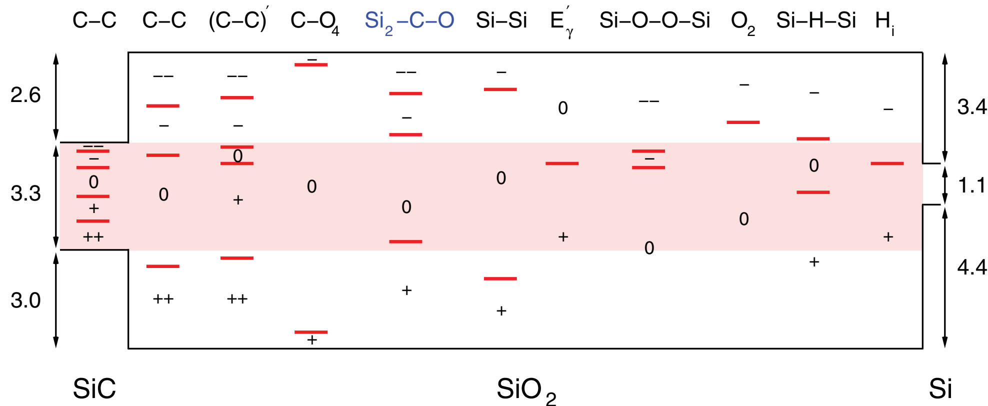

FIG. 24. (Color online) Charge transition levels of several defects calculated in this work in a schematics of the band-gap evolution across the SiC/SiO_2 interface. The positions of the Si band edges are also shown for convenience on the right. The C interstitial (C-C) is found in the SiC substrate. The defects in the SiO_2 oxide comprise two different configurations of the carbon-pair defect [C-C and (C-C)′], the single-C atom coordinated by 4 O atoms (C-O_4), the Si_2-C-O structure, the Si-Si bond (Si-Si), the peroxy linkage (Si-O-O-Si), and the hydrogen bridge (Si-H-Si). The defect levels of the E'_γ defect, the interstitial oxygen molecule (O_2), and the interstitial H atom (H_i) are taken from Ref. 108. When several configurations result in similar defect levels, only the average value is given. Interface-specific electrostatics corrections are not included. The Si_2-C-O defect is highlighted (blue, gray) because it is identified as a good candidate for the high defect density close to the SiC conduction band.

band gap and are separated by only 1.7 eV. The $0/-1$ charge transition level falls in close proximity of the conduction band of SiC, and this property is not spoiled by the consideration of interface-specific electrostatics. However, the experimentally determined density of defect states within the SiC band gap does not show a peak in correspondence of the calculated $+1/0$ charge transition level of the hydrogen bridge defect. The hydrogen bridge defect can therefore not be invoked as the main origin of the high density of defect states just below the conduction band, which is experimentally characterized by a unique sharp peak.

Hydrogen also occurs in the interstitial form in SiO_2. This defect has been the object of numerous investigations and corresponds to an amphoteric defect, which is either found in the positive or negative charge state.[74,91,106,108,117–119] Using the same approach as in this work, previous studies situate the $+1/-1$ charge transition level at 5.6 eV from the valence-band edge of SiO_2,[74,108,117] i.e., in the band gap of SiC at 0.7 eV from the conduction-band edge. This result is in substantial agreement with previous results at the semilocal level, which found the $+1/-1$ level at 3.43 eV in α-cristobalite (Ref. 118) and at 3.25 eV in amorphous SiO_2 (Ref. 91), provided the valence-band edge is shifted downward by 2.5 eV to correct for the band-gap underestimation.[69,75] We note that this $+1/-1$ charge transition level is not subject to electrostatics corrections (cf. Sec. II E). We conclude that the location is too low in the band gap of SiC to match the high defect density in the vicinity of the conduction band of SiC.

VI. CONCLUSIONS

We investigated several candidate defects at the SiC/SiO_2 interface with the main aim of identifying the origin of the large increase in the defect density observed experimentally at the conduction-band edge of SiC. We resorted to a scheme based on hybrid density functionals in order to overcome the band-gap underestimation of semilocal functionals, which would prevent an unambiguous comparison between theory and experiment. Indeed, the identification of typical near-interface defects is expected to mainly rest on the position of energy levels with respect to the relevant band edges.

Our scheme relies on the use of bulk models for the determination of defect levels and on an alignment procedure relying on an atomistic model interface of the SiC/SiO_2 interface. The validity of this scheme is supported by the calculated band offsets, which are found to agree with their experimental counterparts within 0.1 eV. This level of accuracy for the band diagram at the interface appears to be sufficiently reliable to envisage the identification of defect states through a match between calculated and measured energy levels.

In Fig. 24, we give a comprehensive description of the energy levels of the main defects addressed in this work. For completeness, we also include some oxide defects studied previously in Ref. 108 within the same theoretical scheme as used in this work.

Carbon interstitial defects in the SiC substrate (C-C) give charge transition levels that span the whole band gap of SiC, in accord with previous studies based on Kohn-Sham energy levels.[51,53] Hence, this kind of carbon-related defect certainly contributes to the defect density in the band gap of SiC, but the correlation between higher- and lower-lying defect levels makes it an inadequate candidate for the NITs observed close to the conduction band of SiC.

We also considered carbon-pair defects on the SiO_2 side of the interface. We studied two configurations in which the C-C pair is coordinated by Si atoms [C-C and (C-C)′]. These configurations are found to behave differently upon charging due to the amorphous structure of the oxide, and lead to different distributions of defect levels. When the chemical nature of the first neighbors is varied, the energy levels are expected to shift upward,[53] leading to broad distributions. The

broad nature of this defect distribution is incompatible with the sharp peak of the NIT states.

Two single-carbon atom defects in SiO_2 were considered. The C-O_4 defect model, in which a carbon atom replaces a silicon atom of the SiO_2 network, does not give rise to any charge transition level in the SiC band gap. At variance, the Si_2-C-O structure, in which a CO unit substitutes an oxygen atom in a Si-O-Si linkage, features charge transition levels lying close to the valence and conduction bands of SiC. The Si_2-C-O defect could therefore present an electron trap level in correspondence of the experimentally observed NIT levels, while the detection of the associated donor state would be prevented due to its proximity to the valence band of SiC.

Among the oxygen-related defects, we studied defects arising from both oxygen deficiency and oxygen excess. The Si-Si bond defect reveals two charge transition levels far away from the SiC band gap. This defect is therefore not expected to contribute to the $D_{\rm it}$ in the SiC band gap. The E'_γ variant of the oxygen vacancy instead gives a state in the SiC band gap,[108] but its position does not correspond closely to those of the observed NITs.

Upon oxidation, oxygen penetrates into the substrate. We considered the Si-O-C structure, in which an oxygen atom incorporates a Si-C bond of the SiC substrate. As another possibility, we considered a model structure in which a carbon atom of the SiC substrate is replaced by two regular Si-O-Si linkages. None of these oxidized structures gives any defect level in the SiC band gap (not shown in Fig. 24). We then modeled the peroxy linkage (Si-O-O-Si), finding two defect levels in the upper part of the SiC band gap. However, these levels appear too low to originate the experimental NIT peak. The interstitial O_2 molecule (O_2) was discussed as it shows a charge transition level in the vicinity of the conduction-band edge of SiC,[108] but was discarded as origin of the NITs because of its weak bonding to the network structure.[65,90]

Finally, our study concludes with the consideration of hydrogen-related defects. We took under consideration the hydrogen bridge defect, in which a hydrogen atom bridges two silicon atoms in SiO_2 (Si-H-Si) and the interstitial hydrogen defect (H_i). The hydrogen bridge defect has a defect level in the close vicinity of the SiC conduction band, where the NITs show a sharp peak. However, the same defect also shows another defect level much deeper within the band gap of SiC, which dismisses it as a contributor to the NITs. The hydrogen interstitial is also ruled out since it gives a single defect level well within the band gap of SiC.[108]

In conclusion, this study comprises a detailed analysis of the charge transition levels of several defects that could occur at the SiC/SiO_2 interface. Among the defects studied in this work, the features of the Si_2-C-O structure provide the best match with those of the experimentally observed NITs, which are responsible for the high defect density close to the conduction-band edge of SiC.

ACKNOWLEDGMENTS

We acknowledge useful interactions with V. V. Afanas'ev, P. Deák, S. Dhar, L. C. Feldman, E. L. Garfunkel, and H. Ö. Ólafsson. Partial support from the Swiss National Science Foundation is acknowledged (Grant No. 200020-111747). Most of the calculations were performed on the BlueGene computer of EPFL. We also used the cluster PLEIADES-EPFL and other computational facilities at DIT-EPFL, CSEA-EPFL, and CSCS.

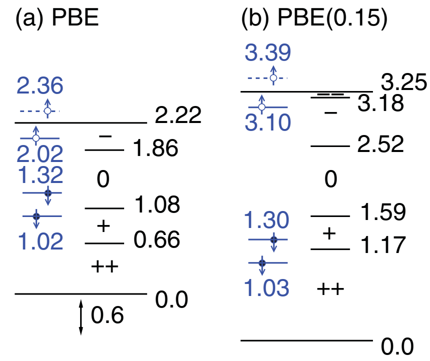

FIG. 25. (Color online) Comparison of the positions of the Kohn-Sham energy levels (black) and their corresponding charge transition levels [blue (gray)] in the (C-C)$_{\rm SiC}$ structure at the (a) PBE and (b) PBE(0.15) levels of theory. The band structures are aligned through the electrostatic potential. The relative positions of the valence-band edges obtained with the different functionals are indicated. Energies are given in eV.

APPENDIX: KOHN-SHAM ENERGY LEVELS VERSUS CHARGE TRANSITION LEVELS

Figures 25 and 26 show the comparison between the positions of the Kohn-Sham energy levels and their corresponding charge transition levels in the (C-C)$_{\rm SiC}$ structure and in the (C-C)$_{\rm SiO_2}$ structure, respectively. The different behavior of the Kohn-Sham energy levels and the charge transition levels upon incorporation of a fraction of nonlocal Fock exchange is noticeable. The occupied Kohn-Sham energy levels tend to follow the evolution of the valence band, while the unoccupied

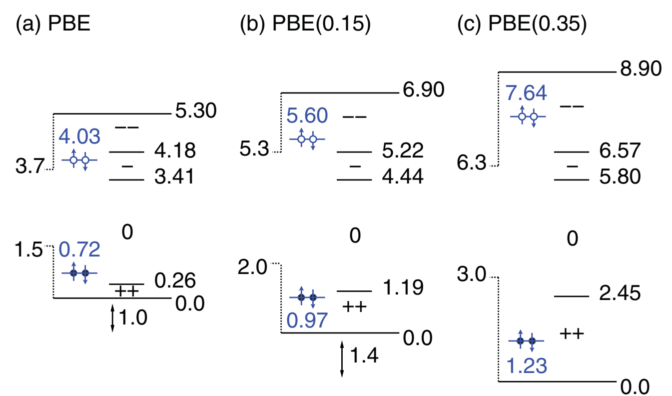

FIG. 26. (Color online) Comparison of the positions of the Kohn-Sham energy levels (black) and their corresponding charge transition levels [blue (gray)] in the (C-C)$_{\rm SiO_2}$ structure at the (a) PBE, (b) PBE(0.15), and (c) PBE(0.35) levels of theory. The position of the SiC band extrema are shown. The band structures are aligned through the electrostatic potential. In (a) and (b), the valence-band edges of SiC are obtained consistently within the respective functionals. In (c), the alignment procedure described in Sec. II C is used. Energies are given in eV.

Kohn-Sham energy levels follow the conduction band. On the other hand, the charge transition levels do not vary when referred to the electrostatic potential. This leads to charge transition levels being up to 1.2 and 1.8 eV below the corresponding Kohn-Sham levels at the PBE(0.15) and PBE(0.35) levels of theory, respectively. Overall, the large variations of the Kohn-Sham energy levels with the functional used indicate that they can not be used to describe accurately the electronic structure of defects. However, they constitute an adequate step to get a qualitative picture from which trends can be extracted. In the present case, the comparison between the positions of the Kohn-Sham energy levels and their corresponding charge transition levels indicates that the C-C pair defects featuring unoccupied Kohn-Sham energy levels above the SiC conduction band are expected to have $0/-1$ and $-1/-2$ charge transition levels in the upper part of the SiC band gap (cf. Fig. 26). This confirms that the Kohn-Sham energy levels can not be used to describe accurately the electronic structure of defects, but can provide useful indications in the investigation of defects.

[1] Yoon Soo Park, in *SiC Materials and Devices*, edited by R. K. Willardson and E. R. Weber (Academic, New York, 1998).
[2] L. A. Lipkin and J. W. Palmour, J. Electron. Mater. **25**, 909 (1996).
[3] H. Li, S. Dimitrijev, H. Harrison, and D. Sweatman, Appl. Phys. Lett. **70**, 2028 (1997).
[4] V. V. Afanasev, M. Bassler, G. Pensl, and M. J. Schulz, Phys. Status Solidi A **162**, 321 (1997).
[5] V. V. Afanas'ev and A. Stesmans, Phys. Rev. Lett. **80**, 5176 (1998).
[6] V. V. Afanas'ev, A. Stesmans, F. Ciobanu, G. Pensl, K. Y. Cheong, and S. Dimitrijev, Appl. Phys. Lett. **82**, 568 (2003).
[7] G. Y. Chung, C. C. Tin, J. R. Williams, K. McDonald, M. Di Ventra, S. T. Pantelides, L. C. Feldman, and R. A. Weller, Appl. Phys. Lett. **76**, 1713 (2000).
[8] N. S. Saks, S. S. Mani, and A. K. Agarval, Appl. Phys. Lett. **76**, 2250 (2000).
[9] H. Kobayashi, T. Sakurai, M. Takahashi, and Y. Nishioka, Phys. Rev. B **67**, 115305 (2003).
[10] J. L. Cantin, H. J. von Bardeleben, Y. Shishkin, Y. Ke, R. P. Devaty, and W. J. Choyke, Phys. Rev. Lett. **92**, 015502 (2004).
[11] V. V. Afanas'ev, A. Stesmans, and C. Harris, Mater. Sci. Forum **264**, 857 (1998).
[12] K.-C. Chang, N. T. Nuhfer, L. M. Porter, and Q. Wahab, Appl. Phys. Lett. **77**, 2186 (2000).
[13] W. Lu, L. C. Feldman, Y. Song, S. Dhar, W. E. Collins, W. C. Mitchel, and J. R. Williams, Appl. Phys. Lett. **85**, 3495 (2004).
[14] C. Castiglioni, C. Mapelli, F. Negri, and G. Zerbi, J. Chem. Phys. **114**, 963 (2001).
[15] C. Virojanadara and L. I. Johansson, Surf. Sci. Lett. **472**, L145 (2001).
[16] C. Virojanadara and L. I. Johansson, Surf. Sci. **505**, 358 (2002).
[17] B. Hornetz, M.-J. Michel, and J. Halbritter, J. Mater. Res. **9**, 3088 (1994).
[18] G. G. Jernigan, R. E. Stahlbush, and N. S. Saks, Appl. Phys. Lett. **77**, 1437 (2000).
[19] J. Dekker, K. Saarinen, H. Ólafsson, and E. Ö. Sveinbjörnsson, Appl. Phys. Lett. **82**, 2020 (2003).
[20] V. V. Afanas'ev and A. Stesmans, Appl. Phys. Lett. **69**, 2252 (1996).
[21] V. V. Afanas'ev and A. Stesmans, Phys. Rev. Lett. **78**, 2437 (1997).
[22] V. V. Afanas'ev, A. Stesmans, M. Bassler, G. Pensl, and M. J. Schulz, Appl. Phys. Lett. **76**, 336 (2000).
[23] V. V. Afanas'ev and A. Stesmans, Appl. Phys. Lett. **71**, 3844 (1997).
[24] R. Schörner, P. Friedrichs, D. Peters, and D. Stephani, IEEE Electron Device Lett. **20**, 241 (1999).
[25] P. Deák, A. Gali, Z. Hajnal, Th. Frauenheim, N. T. Son, E. Janzén, W. J. Choyke, and P. Ordejón, Mater. Sci. Forum **433–436**, 535 (2003).
[26] H. Ö. Ólafsson, E. Ö. Sveinbjörnsson, T. E. Rudenko, I. P. Tyagulski, I. N. Osiyuk, and V. S. Lysenko, Appl. Phys. Lett. **79**, 4034 (2001).
[27] H. Ö. Ólafsson, F. Allerstam, and E. Ö. Sveinbjörnsson, Mater. Sci. Forum **389–393**, 1005 (2002).
[28] E. Pippel, J. Woltersdorf, H. Ö. Ólafsson, and E. Ö. Sveinbjörnsson, J. Appl. Phys. **97**, 034302 (2005).
[29] H. Ö. Ólafsson, E. Ö. Sveinbjörnsson, T. E. Rudenko, V. I. Kilchytska, I. P. Tyagulski, and I. N. Osiyuk, Mater. Sci. Forum **433–436**, 547 (2003).
[30] X. D. Chen, S. Dhar, T. Isaacs-Smith, J. R. Williams, L. C. Feldman, and P. M. Mooney, J. Appl. Phys. **103**, 033701 (2008).
[31] S. Dhar, X. D. Chen, P. M. Mooney, J. R. Williams, and L. C. Feldman, Appl. Phys. Lett. **92**, 102112 (2008).
[32] K. McDonald, R. A. Weller, S. T. Pantelides, L. C. Feldman, G. Y. Chung, C. C. Tin, and J. R. Williams, J. Appl. Phys. **93**, 2719 (2003).
[33] P. Jamet and S. Dimitrijev, Appl. Phys. Lett. **79**, 323 (2001).
[34] P. T. Lai, S. Chakraborty, C. L. Chan, and Y. C. Cheng, Appl. Phys. Lett. **76**, 3744 (2000).
[35] S. Dhar, L. C. Feldman, S. Wang, T. Isaacs-Smith, and J. R. Williams, J. Appl. Phys. **98**, 014902 (2005).
[36] J. P. Xu, P. T. Lai, C. L. Chan, B. Li, and Y. C. Cheng, IEEE Electron Device Lett. **21**, 298 (2000).
[37] G. Gudjónsson, H. Ö. Ólafsson, and E. Ö. Sveinbjörnsson, Mater. Sci. Forum **457–460**, 1425 (2004).
[38] H. Yano, F. Furumoto, T. Niwa, T. Hatayama, Y. Uraoka, and T. Fuyuki, Mater. Sci. Forum **457–460**, 1333 (2004).
[39] F. Ciobanu, G. Pensl, V. Afanas'ev, and A. Schörner, Mater. Sci. Forum **483–485**, 693 (2005); F. Ciobanu, T. Franck, G. Pensl, V. Afanas'ev, S. Shamuilia, A. Schörner, and T. Kimoto, *ibid.* **527–529**, 991 (2006).
[40] S. Dhar, L. C. Feldman, S. Wang, T. Isaacs-Smith, and J. R. Williams, J. Appl. Phys. **98**, 014902 (2005); S. Dhar, S. Wang, A. C. Ahyi, T. Isaacs-Smith, S. T. Pantelides, J. R. Williams, and L. C. Feldman, Mater. Sci. Forum **527–529**, 949 (2006).
[41] S. T. Pantelides, S. Wang, A. Franceschetti, R. Buczko, M. Di Ventra, S. N. Rashkeev, L. Tsetseris, M. H. Evans, I. G. Batyrev, L. C. Feldman, S. Dhar, K. McDonald, R. A. Weller, R. D. Scrimpf, D. M. Fleetwood, X. J. Zhou, J. R. Williams, C. C. Tin, G. Y.

Chung, T. Isaacs-Smith, S. R. Wang, S. J. Pennycook, G. Duscher, K. van Benthem, and L. M. Porter, Mater. Sci. Forum **527–529**, 935 (2006).
[42]P. Deák, J. M. Knaup, T. Hornos, C. Thill, A. Gali, and T. Frauenheim, J. Phys. D: Appl. Phys. **40**, 6242 (2007).
[43]K.-C. Chang, L. M. Porter, J. Bentley, C.-Y. Lu, and Jr J. Cooper, J. Appl. Phys. **95**, 8252 (2004).
[44]P. Jamet, S. Dimitrijev, and P. Tanner, J. Appl. Phys. **90**, 5058 (2001).
[45]F. Allerstam, G. Gudjónsson, H. Ö. Ólafsson, E. Ö. Sveinbjörnsson, T. Rödle, and R. Jos, Mater. Sci. Forum **483–485**, 837 (2005).
[46]M. K. Das, B. A. Hull, S. Krishnaswami, F. Husna, S. Haney, A. Lelis, C. J. Scozzie, and J. D. Scofield, Mater. Sci. Forum **527–529**, 967 (2006).
[47]E. Ö. Sveinbjörnsson, G. Gudjónsson, F. Allerstam, H. Ö. Ólafsson, P.-Å. Nilsson, H. Zirath, T. Rödle, and R. Jos, Mater. Sci. Forum **527–529**, 961 (2006).
[48]E. Ö. Sveinbjörnsson, F. Allerstam, H. Ö. Ólafsson, G. Gudjónsson, D. Dochev, T. Rödle, and R. Jos, Mater. Sci. Forum **556–557**, 487 (2007).
[49]G. Gudjónsson, H. Ö. Ólafsson, F. Allerstam, P.-Å. Nilsson, E. Ö. Sveinbjörnsson, T. Rödle, and R. Jos, Mater. Sci. Forum **483–485**, 833 (2005).
[50]J. M. Knaup, P. Deák, Th. Frauenheim, A. Gali, Z. Hajnal, and W. J. Choyke, Phys. Rev. B **71**, 235321 (2005).
[51]J. M. Knaup, P. Deák, Th. Frauenheim, A. Gali, Z. Hajnal, and W. J. Choyke, Phys. Rev. B **72**, 115323 (2005).
[52]S. Wang, S. Dhar, S. R. Wang, A. C. Ahyi, A. Franceschetti, J. R. Williams, L. C. Feldman, and S. T. Pantelides, Phys. Rev. Lett. **98**, 026101 (2007).
[53]F. Devynck, A. Alkauskas, P. Broqvist, and A. Pasquarello, Phys. Rev. B **83**, 195319 (2011).
[54]J. P. Perdew, M. Ernzerhof, and K. Burke, J. Chem. Phys. **105**, 9982 (1996).
[55]A. Alkauskas, P. Broqvist, F. Devynck, and A. Pasquarello, Phys. Rev. Lett. **101**, 106802 (2008).
[56]F. Devynck, F. Giustino, P. Broqvist, and A. Pasquarello, Phys. Rev. B **76**, 075351 (2007).
[57]F. Devynck, A. Alkauskas, P. Broqvist, and A. Pasquarello, AIP Conf. Proc. **1199**, 108 (2009).
[58]J. P. Perdew, K. Burke, and M. Ernzerhof, Phys. Rev. Lett. **77**, 3865 (1996).
[59]N. Troullier and J. L. Martins, Phys. Rev. B **43**, 1993 (1991).
[60]J. Muscat, A. Wander, and N. M. Harrison, Chem. Phys. Lett. **342**, 397 (2001).
[61]J. Heyd, J. E. Peralta, G. E. Scuseria, and R. L. Martin, J. Chem. Phys. **123**, 174101 (2005).
[62]P. Broqvist, A. Alkauskas, and A. Pasquarello, Phys. Rev. B **80**, 085114 (2009); **81**, 039903(E) (2010).
[63]CPMD. v3.11.1, Copyright IBM Corp 1990-2006, Copyright MPI. für Festkörperforschung Stuttgart 1997-2001; J. Hutter and A. Curioni, ChemPhysChem **6**, 1788 (2005).
[64]J. Sarnthein, A. Pasquarello, and R. Car, Phys. Rev. Lett. **74**, 4682 (1995); Phys. Rev. B **52**, 12690 (1995).
[65]A. Bongiorno and A. Pasquarello, Phys. Rev. Lett. **88**, 125901 (2002).
[66]F. Mauri, A. Pasquarello, B. G. Pfrommer, Y.-G. Yoon, and S. G. Louie, Phys. Rev. B **62**, R4786 (2000).
[67]C. G. Van de Walle and R. M. Martin, Phys. Rev. B **34**, 5621 (1986).
[68]A. Baldereschi, S. Baroni, and R. Resta, Phys. Rev. Lett. **61**, 734 (1988).
[69]A. Alkauskas, P. Broqvist, and A. Pasquarello, Phys. Rev. Lett. **101**, 046405 (2008).
[70]A. Alkauskas, P. Broqvist, and A. Pasquarello, Phys. Status Solidi B **248**, 775 (2011).
[71]J. Godet, P. Broqvist, and A. Pasquarello, Appl. Phys. Lett. **91**, 262901 (2007).
[72]P. Broqvist, A. Alkauskas, and A. Pasquarello, Appl. Phys. Lett. **92**, 132911 (2008).
[73]A. Alkauskas, P. Broqvist, and A. Pasquarello, Phys. Rev. B **78**, 161305(R) (2008).
[74]P. Broqvist, A. Alkauskas, J. Godet, and A. Pasquarello, J. Appl. Phys. **105**, 061603 (2009).
[75]P. Dahinden, P. Broqvist, and A. Pasquarello, Phys. Rev. B **81**, 085331 (2010).
[76]P. Broqvist, A. Alkauskas, and A. Pasquarello, Phys. Status Solidi A **2007**, 270 (2010).
[77]P. Broqvist, J. F. Binder, and A. Pasquarello, Appl. Phys. Lett. **97**, 202908 (2010).
[78]D. R. Franceschetti, Solid State Ionics **2**, 39 (1981).
[79]Y. Deng, W. Wang, Q. Fang, M. B. Koushik, and T. P. Chow, J. Electron. Mater. **35**, 618 (2006).
[80]C. G. Van de Walle and J. Neugebauer, J. Appl. Phys. **95**, 3851 (2004).
[81]C. W. M. Castleton, A. Höglund, and S. Mirbt, Phys. Rev. B **73**, 035215 (2006).
[82]G. Makov and M. C. Payne, Phys. Rev. B **51**, 4014 (1995).
[83]S. Lany and A. Zunger, Phys. Rev. B **78**, 235104 (2008).
[84]C. Freysoldt, J. Neugebauer, and C. G. Van de Walle, Phys. Rev. Lett. **102**, 016402 (2009).
[85]S. E. Taylor and F. Bruneval, Phys. Rev. B **84**, 075155 (2011).
[86]H.-P. Komsa and A. Pasquarello, Phys. Rev. B **84**, 075207 (2011).
[87]P. Broqvist, A. Alkauskas, and A. Pasquarello, Phys. Rev. B **78**, 075203 (2008).
[88]M. A. Szymanski, A. L. Shluger, ans A. M. Stoneham, Phys. Rev. B **63**, 224207 (2001).
[89]S. Mukhopadhyay, P. V. Sushko, A. M. Stoneham, and A. L. Shluger, Phys. Rev. B **70**, 195203 (2004).
[90]A. Bongiorno and A. Pasquarello, Phys. Rev. B **70**, 195312 (2004).
[91]J. Godet and A. Pasquarello, Microelectron. Eng. **80**, 288 (2005).
[92]P. Broqvist and A. Pasquarello, Microelectron. Eng. **84**, 2022 (2007).
[93]F. Giustino, P. Umari, and A. Pasquarello, Phys. Rev. Lett. **91**, 267601 (2003).
[94]F. Giustino and A. Pasquarello, Phys. Rev. B **71**, 144104 (2005).
[95]F. Devynck and A. Pasquarello, Phys. B (Amsterdam) **401–402**, 556 (2007).
[96]H.-P. Komsa, P. Broqvist, and A. Pasquarello, Phys. Rev. B **81**, 205118 (2010).
[97]A. Alkauskas and A. Pasquarello, Phys. Rev. B **84**, 125206 (2011).
[98]The $E^{-1/-2}$ level had not been identified in Ref. 57.
[99]X. Shen and S. T. Pantelides, Appl. Phys. Lett. **98**, 053507 (2011).
[100]A. Gali, P. Deák, P. Ordejón, N. T. Son, E. Janzén, and W. J. Choyke, Phys. Rev. B **68**, 125201 (2003).
[101]S. Wang, M. Di Ventra, S. G. Kim, and S. T. Pantelides, Phys. Rev. Lett. **86**, 5946 (2001).
[102]V. V. Afanas'ev, A. Stesmans, M. Bassler, G. Pensl, M. J. Schulz, and C. I. Harris, J. Appl. Phys. **85**, 8292 (1999).

[103]For 0/ − 1 vertical transitions, we used a Makov-Payne correction (Ref. 82) of 0.95 eV corresponding to an ion-clamped dielectric constant of 2.1 for SiO_2. In the Lany-Zunger correction scheme (Ref. 83), the calculated transitions would be found at energies lower by 0.3 eV.
[104]H. Watanabe, T. Hosoi, T. Kirino, Y. Kagei, Y. Uenishi, A. Chanthaphan, A. Yoshigoe, Y. Teraoka, and T. Shimura, Appl. Phys. Lett. **99**, 021907 (2011).
[105]A. Bongiorno and A. Pasquarello, Phys. Rev. B **62**, 16326(R) (2000).
[106]P. E. Blöchl, Phys. Rev. B **62**, 6158 (2000).
[107]C. M. Carbonaro, V. Fiorentini, and F. Bernardini, Phys. Rev. Lett. **86**, 3064 (2001).
[108]A. Alkauskas, P. Broqvist, and A. Pasquarello, AIP Conf. Proc. **1199**, 79 (2009).
[109]J. K. Rudra and W. B. Fowler, Phys. Rev. B **35**, 8223 (1987).
[110]D. C. Allan and M. P. Teter, J. Am. Ceram. Soc. **73**, 3247 (1990).
[111]M. Boero, A. Pasquarello, J. Sarnthein, and R. Car, Phys. Rev. Lett. **78**, 887 (1997).
[112]D. R. Hamann, Phys. Rev. Lett. **81**, 3447 (1998).
[113]Y.-G. Jin and K.-J. Chang, Phys. Rev. Lett. **86**, 1793 (2001).
[114]A. M. Stoneham, M. A. Szymanski, and A. Shluger, Phys. Rev. B **63**, 241204(R) (2001); M. A. Szymanski, A. M. Stoneham, and A. Shluger, Microelectron. Reliab. **40**, 567 (2000).
[115]A. Bongiorno and A. Pasquarello, J. Phys.: Condens. Matter **17**, S2051 (2005).
[116]A. Bongiorno and A. Pasquarello, Solid-State Electron. **46**, 1873 (2002).
[117]A. Alkauskas and A. Pasquarello, Phys. B (Amsterdam) **401–402**, 546 (2007).
[118]A. Yokozawa and Y. Miyamoto, Phys. Rev. B **55**, 13783 (1997).
[119]P. E. Bunson, M. Di Ventra, S. T. Pantelides, R. D. Schrimpf, and K. F. Galloway, IEEE Trans. Nucl. Sci. **46**, 1568 (1999).